Atmos. Chem. Phys. Discuss., 11, 2991–3040, 2011
www.atmos-chem-phys-discuss.net/11/2991/2011/
doi:10.5194/acpd-11-2991-2011

Atmospheric Chemistry and Physics Discussions

Hygroscopic properties of aerosol particles at high relative humidity and their diurnal variations in the North China Plain

P. F. Liu[1], C. S. Zhao[1], T. Göbel[2], E. Hallbauer[2], A. Nowak[2], L. Ran[1], W. Y. Xu[1], Z. Z. Deng[1], N. Ma[1], K. Mildenberger[2], S. Henning[2], F. Stratmann[2], and A. Wiedensohler[2]

[1]Department of Atmospheric and Oceanic Sciences, School of Physics, Peking University, Beijing, 100871, China
[2]Institute for Tropospheric Research, Permoserstr. 15, 04318 Leipzig, Germany

Received: 5 January 2011 – Accepted: 12 January 2011 – Published: 26 January 2011

Correspondence to: C. S. Zhao (zcs@pku.edu.cn)

Published by Copernicus Publications on behalf of the European Geosciences Union.

Abstract

The hygroscopic properties of submicron aerosol particles were determined at a suburban site (Wuqing) in the North China Plain among a cluster of cities during the period 17 July to 12 August 2009. A High Humidity Tandem Differential Mobility Analyser (HH-TDMA) instrument was applied to measure the hygroscopic growth factor (GF) at 90%, 95% and 98.5% relative humidity (RH) for particles with dry diameter between 50–250 nm. The probability distribution of GF (GF-PDF) averaged over the period shows a distinct bimodal pattern, namely, a dominant more-hygroscopic (MH) group and a smaller nearly-hydrophobic (NH) group. The MH group particles were highly hygroscopic, and their GF was relatively constant during the period with average values of 1.54 ± 0.02, 1.81 ± 0.04 and 2.45 ± 0.07 at 90%, 95% and 98.5% RH ($D_0 = 100$ nm), respectively. The NH group particles grew very slightly when exposed to high RH, with GF values of 1.08 ± 0.02, 1.13 ± 0.06 and 1.24 ± 0.13, respectively at 90%, 95% and 98.5% RH ($D_0 = 100$ nm). The hygroscopic growth behaviours at different RHs were well represented by the hygroscopicity parameter κ with a single-parameter Köhler model. Thus, the calculation of GF as a function of RH and dry diameter could be facilitated by an empirical parameterization of κ as function of dry diameter. A strong diurnal pattern in number fraction of different hygroscopic groups was observed, indicating a diurnal variation of aerosol mixing state and/or chemical composition. The average number fraction of NH particles during the day was about 8%, while during the nighttime fractions up to 20% were reached. Correspondingly, the state of mixing in terms of water uptake varied significantly during a day. The high fraction of NH particles measured during the night denotes a high degree of external mixing of ambient aerosols, while during the day the degree of external mixing decreased. Simulations using a particle-resolved aerosol box model (PartMC-MOSAIC) suggest that the diurnal variations of aerosol hygroscopicity and mixing state were mainly caused by the evolution of the atmospheric mixing layer. The shallow nocturnal boundary layer during the night facilitated the accumulation of freshly emitted carbonaceous particles (mainly

ACPD
11, 2991–3040, 2011

hydrophobic) near the surface while in the morning turbulence entrained the more aged and more hygroscopic particles from aloft and diluted the NH particles near the surface resulting in a decrease in the fraction of NH particles.

1 Introduction

The North China Plain is a polluted area with great industrial activity and dense population. A group of megacities (so-called city cluster) including Beijing and Tianjin is located in this region. Along with the rapid economic growth and increase in traffic during the last decades, the consumption of fossil fuels like coal, gasoline, diesel and natural gas has increased dramatically in China. The combustion of fossil fuels emits large amounts of particulate and gaseous pollutants into the atmosphere, leading to substantial environmental problems. Industrial and traffic related primary emissions, as well as the formation of secondary aerosols, combined with the transport of dust from the desert region, result frequently in heavy aerosol loads in this area depending on the meteorological conditions (Wehner et al., 2004, 2008; Liu et al., 2009). Air quality is significantly influenced by aerosol particles and high loads of aerosol pollution severely degrade visibility, especially at high RH in summer (Zhang et al., 2010); related health risks are increased as well (Leitte, 2011). Moreover, aerosol particles influence the earth's radiative budget directly by scattering and absorbing solar radiation (Charlson et al., 1992), and indirectly by serving as nuclei for cloud formation (Twomey, 1974; Albrecht, 1989). Aerosols may also affect the hydrological cycle (Menon et al., 2002). A study shows that the magnitude of precipitation in the North China Plain has decreased significantly during the last 40 years and that the reduction of precipitation is strongly correlated to the high concentration of aerosol particles (Zhao et al., 2006b).

In order to reduce the uncertainties in model projections of climate change induced by aerosol indirect effects, intensive aircraft measurement studies on warm cloud microphysical properties were conducted in the areas of high aerosol loading, such as the North China Plain (Zhao et al., 2006a; Deng et al., 2009). To understand the aerosol

ACPD
11, 2991–3040, 2011

effects on climate via their effects on clouds, the aerosol hygroscopic properties are very crucial since they describe the interactions of aerosol particles with water vapour which are closely related to the cloud condensation nuclei (CCN) activity of aerosol particles (Swietlicki et al., 2008) and their number-size distribution.

Moreover, hygroscopic particles grow significantly in size at high RH (but less than 100%) due to water uptake, hence influence the aerosol optical properties, such as extinction, visibility and aerosol optical depth (AOD) (Cheng et al., 2008). Inadequate characterization of aerosol hygroscopic properties will induce large uncertainties in the estimation of aerosol direct effect on the climate.

Hygroscopic properties of aerosol particles can be determined by their physical and chemical characteristics (Topping et al., 2005a, b). The Köhler equation is often used to describe both the hygroscopic growth and the activation of aerosol particles to cloud droplets, based on the aerosol's physicochemical properties (Köhler, 1936). However, these detailed properties are not always available for ambient aerosols. Size-dependent mixing states of various chemical compositions also increase the complexity. Recently, several single-parameter schemes have been proposed to simplify the Köhler equation. Hygroscopicity parameters such as κ and ρ_{ion} have been defined as proxies of chemical composition to represent aerosol hygroscopicity (Petters and Kreidenweis, 2007; Wex et al., 2007). It is worth noting that the hygroscopicity parameter for the Köhler model is not always a constant with respect to RH, especially for the range of RH above 90%. Laboratory studies using LACIS (Leipzig Aerosol Cloud Interaction Simulator) observed an increased hygroscopicity parameter by a factor of 4–6 for secondary organic aerosol (SOA) in the RH-range from below 90% to 99.6% (Wex et al., 2009; Petters et al., 2009). The RH-dependence of κ could be crucial for the prediction of CCN activity. For ambient aerosols, validations of the applicability of single-parameter simplification at RH above 90% through field measurements are necessary and are rarely reported in the current literature (Mildenberger et al., 2011).

ACPD
11, 2991–3040, 2011

Ambient aerosols are external and internal mixtures of particles with different chemical compounds such as soot, sulphate, nitrate, organic carbon and mineral dust. The state of mixing of these components is crucial for understanding the role of aerosol particles in the atmosphere. In recent years, much attention has been paid to the mixing state of soot in aerosols (Jacobson, 2001; Moffet and Prather, 2009; Riemer et al., 2009; Zhang et al., 2008; Oshima et al., 2009), which influences the optical properties and climate effects of aerosols. A Humidified Tandem Differential Mobility Analyser (H-TDMA) is one of the few instruments capable of providing information regarding the mixing state in terms of hygroscopicity of the atmospheric aerosols (Swietlicki et al., 2008). The heterogeneous mixtures of chemical components reveal different hygroscopicity and CCN activity (Riemer et al., 2010); hence detailed hygroscopic properties provide important information on the aerosol mixing state. Different modes of hygroscopic growth of ambient aerosols are often observed in the H-TDMA measurements, indicating an external mixture in terms of hygroscopicity (Swietlicki et al., 2008).

A large number of ship- and ground-based measurements for the size-resolved hygroscopic properties of ambient aerosols have been conducted worldwide using the H-TDMA technique of which the results were summarized in a review paper by Swietlicki et al. (2008). In the North China Plain area, Massling et al. (2009) and Meier et al. (2009) recently reported the hygroscopic properties measured in Beijing city using various instruments including the H-TDMA. However, due to technical limitations, most of these conventional H-TDMA field studies were conducted at the RH ranges below 90%. Detailed hygroscopic properties of atmospheric aerosols at RHs above 90% are still very scarce. Considering that the hygroscopic growth factors at high RH are highly sensitive to aerosol chemical composition and are more closely related to cloud droplet activation behaviours, there is a strong need to measure the detailed hygroscopic properties for ambient aerosols at RH above 90%.

In this paper, we focus on measurement of the aerosol hygroscopic properties in a polluted megacity area at RH values above 90%. The High Humidity Tandem Differential Mobility Analyser (HH-TDMA) developed by Hennig et al. (2005) was applied in

ACPD
11, 2991–3040, 2011

the field study to determine the hygroscopic properties of ambient aerosols at 90%, 95% and 98.5% RH. The hygroscopic growth factors and number fractions of different hygroscopic groups are analysed. The calculated hygroscopicity parameters, κ, are presented in this paper as well, and the size-dependent κ values are parameterized to facilitate the application of our result in models. The diurnal variations of aerosol mixing state revealed by detailed hygroscopic properties are also discussed, and these diurnal patterns are interpreted by modelling simulations using a state-of-the-art, particle-resolved aerosol box model PartMC-MOSAIC developed by Riemer et al. (2009).

2 Data and methods

2.1 Description of the measurement campaign

This investigation is part of the project HaChi (Haze in China), which was conducted by the collaboration of Peking University (PKU), China and Leibniz-Institute for Tropospheric Research (IFT), Germany. During an intensive field campaigns in July–August 2009, the aerosol number-size distribution, hygroscopicity, CCN activity, chemical composition and optical properties were measured at ground level. The period of the HH-TDMA measurements analysed in this study is between 17 July 2009 and 12 August 2009, namely, HaChi summer campaign. The HH-TDMA system was located in an air-conditioned mobile laboratory with well controlled room temperature. Air was sampled through a low flow PM_{10} inlet. The aerosol flow was dehumidified to a relative humidity below 30% by an automatic aerosol dryer unit (Tuch et al., 2009) on the roof of the laboratory before it entered the measurement systems.

The measurement site was situated next to the Wuqing Meteorological Station (39°23′ N, 117°01′ E, 7.4 m a.s.l.). The site is located in the west of the town, surrounded by an area with mixed agricultural, residential and industrial land use. Figure 1 shows the location of the measurement site, nearby major cities and the distribution of

ACPD
11, 2991–3040, 2011

4-yr average (2005–2008) AOD derived from the Moderate Resolution Imaging Spectroradiometer (MODIS) at 550 nm wavelength. The contour map of AOD shown in Fig. 1 demonstrates the region of high AOD from the edge of the North China Plain (north and west of Beijing) expanding to the south and east with AOD exceeding 0.6, indicating the heavy pollution in the North China Plain. Around cities such as Beijing (with about 16 million inhabitants), Tianjin (10 million inhabitants) and Baoding (1 million inhabitants) AOD values exceed 0.8 which reflect the major anthropogenic aerosol emissions in these areas. Wuqing is a suburban district of Tianjin (with about 0.8 million inhabitants) located among a cluster of large cities. The urban areas of Beijing and Tianjin are 80 km to the northwest and 30 km to the southeast of Wuqing, respectively. Tangshan (4 million inhabitants) and Baoding are two other cities in the North China Plain 130 km to the northeast and 160 km to the northwest of Wuqing, respectively. The average AOD at Wuqing is about 0.7, which is near the regional average value of the large polluted area in the North China Plain. Therefore, it is an optimal site for field studies which represents an average pollution level for aerosol measurements in the megacity region. The site is thus representative of the regional polluted aerosol in the North China Plain. The site is in the GMT +8:00 time zone. All times in the paper are reported as GMT +8:00.

2.2 Instrumentation and data

2.2.1 HH-TDMA

The main instrument used in this study was a High Humidity Tandem Differential Mobility Analyser (HH-TDMA). The HH-TDMA was designed to measure size-resolved hygroscopic properties for laboratory and ambient aerosol at RHs between 90% and 98.5% (Hennig et al., 2005). The general principle is similar to that of the hygroscopicity tandem mobility analyser system (H-TDMA; Rader and McMurry, 1986). However, in the conventional H-TDMA-system, the temperature fluctuations may cause instabilities of RH in the second DMA. The direct humidification has its technical limit as well.

ACPD
11, 2991–3040, 2011

Due to these limitations, a stable humidification of the aerosol and sheath air is difficult to maintain for RHs above 90%. To measure the aerosol hygroscopicity at high RHs, the set-up of the HH-TDMA-system was re-designed to minimize the temperature fluctuation in the humidification process and in the size distribution measurement.

Similar to the H-TDMA-system, the HH-TDMA consists of two DMAs connected in series with a humidity conditioning section between them. The first DMA extracts a narrow size increment from the ambient polydisperse aerosol and is operated at RH < 5%. This nearly monodisperse aerosol is exposed to a well-defined, higher RH in the humidity conditioning section, and the increase of the particle size due to the water uptake is determined by the second DMA. Different from the conventional H-TDMA, two separate temperature controlled water baths are employed to control the temperature of humidity conditioning section and temperature of the second DMA, respectively. A constant temperature decrease of approximately 2 K is maintained between the second water bath (for the second DMA) and the first water bath (for the humidity conditioning section). The humidity conditioning section can humidify the sheath air and the aerosol flow to RH values lower than 90% (about 77% ~ 83% in this study) by regulated mixing of dry air (<5% RH) and humid air (~95% RH). The final RH, up to 98.5%, is produced by decreasing the temperature of the second DMA relative to the humidity conditioning section. A dew point mirror is located in the excess air line of the second DMA to measure the RH inside. Temperature and RH stability tests conducted by Hennig et al. (2005) showed that the absolute temperatures in HH-TDMA-system can be maintained within ±0.1 K, the stability within ±0.02 K and the RH in the second DMA reaches an absolute accuracy of ±1.2% for 98%. More detailed information regarding the HH-TDMA-system is provided by Hennig et al. (2005).

During the HaChi summer campaign, the RH values of the second DMA were set to be 90%, 95% and 98.5%. The dry diameters selected by the first DMA were set to be 50 nm, 100 nm, 200 nm and 250 nm. For calibration, the growth factors of ammonium sulphate particles with 200 nm dry size at low RH (approximately 22.5% in this study) and at 90%, 95% and 98.5% RH were measured every day. The hygroscopic

ACPD
11, 2991–3040, 2011

behaviour of the ammonium sulphate particles is well depicted by the Köhler theory with a parameterized van't Hoff factor (Low, 1969; Young and Warren, 1992). Since 200 nm ammonium sulphate particles are unable to take up water at RH lower than the deliquescence point (about 80%), the low RH scans were applied to calibrate any possible offset in sizing by the second DMA cf. the first, as well as to determine the TDMA kernel function, which describes the instrument response used in the inversion algorithm (see Gysel et al., 2009). Ammonium sulphate scans at RH values greater than 85% are applied to correct the RH difference between the second DMA and the dew point mirror at high RH range between 90% and 100%. The flows in the HH-TDMA system were checked by a Primary Standard Airflow Calibrator (Gilian Gilibrator) daily during the measurement period. A data quality control routine was designed to check the temperature and RH stabilities of the system, hence exclude any invalid data.

2.2.2 Single-parameter Köhler model

Both the hygroscopic growth and activation behaviours of atmospheric aerosols can be described by the Köhler theory (Köhler, 1936). The Köhler theory considers the Kelvin effect and the Raoult effect, establishing a relationship between the water vapour saturation ratio S over the surface of a droplet and the droplet diameter D:

$$S(D) = a_w \exp\{(4\sigma_{s/a} M_w)/(RT\rho_w D)\} \quad (1)$$

where a_w is the activity of water in solution, ρ_w is the density of water, M_w is the molecular weight of water, $\sigma_{s/a}$ is the surface tension of the solution/air interface, R is the universal gas constant, T is the temperature, and D is the diameter of the droplet. In our study, a simple hygroscopicity parameter is needed to facilitate the comparison of the hygroscopicity of particles with different dry diameters, and at different RHs as well. Several essentially equivalent single parameterizations for Köhler model have been suggested in the literature (Rissler et al., 2006; Petters and Kreidenweis, 2007; Wex et al., 2007). Here, we use hygroscopicity parameter κ (Petters and Kreidenweis,

ACPD
11, 2991–3040, 2011

2007) to analyse our measurement data. The parameter κ is defined by the following expression:

$$a_w = (D^3 - D_0^3)/(D^3 - D_0^3(1-\kappa)) \quad (2)$$

where, D_0 is the dry diameter, $\kappa = (i\rho_s M_w)/(M_s\rho_w)$, with the van't Hoff factor i, density of solute ρ_s and molar mass of solute M_s, respectively. The Köhler curve can be computed by inserting Eq. (2) into Eq. (1):

$$S(D) = (D^3 - D_0^3)/(D^3 - D_0^3(1-\kappa))\exp\{(4\sigma_{s/a}M_w)/(RT\rho_w D)\} \quad (3)$$

The value of κ is obtained from measured RH and hygroscopic growth factor (GF) defined as:

$$\mathrm{GF} = D/D_0 \quad (4)$$

by solving Eq. (1):

$$\kappa(\mathrm{GF}) = (\mathrm{GF}^3 - 1)[\exp\{(4\sigma_{s/a}M_w)/(RT\rho_w \mathrm{GF} D_0)\}/S - 1] \quad (5)$$

Conversely, for a known κ, the GF at any RH could also be derived by solving Eq. (3) numerically. In this study, the temperature used in the κ calculation is 20 °, and the surface tension of the solution/air interface $\sigma_{s/a}$ is assumed to be the same as the surface tension of the pure water/air interface (about 0.0728 N/m at 20 °).

2.2.3 Data analysis and inversion algorithm

The goals of the H-TDMA measurement and data analysis approach are to obtain the probability distribution function of the growth factor (GF-PDF), hence the mean GF and the number fraction (nf) for different growth factor ranges. In the HH-TDMA-system, the number concentration of the selected dry aerosol particles is measured by the first CPC, and the number-size distribution of the humidified aerosol particles is determined using the second DMA and CPC. The measured growth factor distributions can be

ACPD
11, 2991–3040, 2011

calculated by dividing the size of the humidified particle by the size of the dry particle. However, due to the finite widths of the size increments of selected particles with two DMAs, the measured distribution function (MDF) is a skewed and smoothed integral transform of the actual growth factor probability distribution function (GF-PDF, c(GF)) (Gysel et al., 2009). Therefore, a data inversion procedure is needed to retrieve the GF-PDF from the measured data. The TDMAfit algorithm (Stolzenburg and McMurry, 1988) is a widely used approach to invert TMDA data. Recently, Gysel et al. (2009) designed a new data inversion routine (TDMAinv) for the TDMA measurements, which has been applied successfully to ambient H-TDMA data (Gysel et al., 2007; Sjogren et al., 2008). In the TDMAinv algorithm, the GF-PDF is assumed to be a piecewise linear function in fixed growth factor intervals, which can reproduce the MDF with the smallest residual cf. the input MDF. For the TDMAinv algorithm the initial guess for the optimization is not needed, thus it is suitable for analyzing large amounts of data. Here, the TDMAinv algorithm was applied to process the HH-TDMA data. The GF-PDF is retrieved from the TDMAinv algorithm for each measurement and normalized to unity ($\int c(\mathrm{GF}) d\mathrm{GF} = 1$).

Due to a degree of regularity in the complex mixing state of ambient aerosols, different groupings in terms of modes of hygroscopic growth of particles were frequently and repeatedly observed in our field campaigns. Accordingly, we classify the particles into a nearly-hydrophobic (NH) group, a less-hygroscopic (LH) group, and a more-hygroscopic (MH) group. Since the GF are very sensitive to RH, and the curvature effect (Kelvin effect) results in decreasing GF for decreasing particle size, a classification of GF data into different hygroscopic groups needs to take the RH effect and the curvature effect into account to obtain better consistency. Conventionally, the soluble particle volume fraction $\varepsilon_{\mathrm{AS}}$ (using ammonium sulphate as the reference compound) is used to define the boundaries for different groups of hygroscopic growth (Swietlicki et al., 2008, 1999; Svenningsson et al., 1994; Rissler et al., 2006). In this study, we use the parameter κ (defined in Sect. 2.2.2) as an equivalent alternative to establish boundaries for each grouping of hygroscopic growth. The following values of κ have

ACPD
11, 2991–3040, 2011

been determined to be suitable for most of our data to separate the hygroscopic groups (GF values are for 100 nm dry size particles at RH=90%; these values varies at other size or RH):

Nearly-hydrophobic particles (NH): $\kappa <= 0.10$ $(GF <= 1.21)$;

Less-hygroscopic particles (LH): $\kappa = 0.10 - 0.20$ $(GF = 1.21 - 1.37)$;

More-hygroscopic particles (MH): $\kappa > 0.20$ $(GF > 1.37)$

The HH-TDMA data is presented as a HaChi project average of the hygroscopic growth factor ($GF_{NH,LH,MH}$) and number fraction ($nf_{NH,LH,MH}$) for each group, which are calculated using following equations:

$$GF_{NH,LH,MH} = \left(\frac{\int_{GF\_lim1}^{GF\_lim2} GF^3 \cdot c(GF) dGF}{\int_{GF\_lim1}^{GF\_lim2} c(GF) dGF} \right)^{1/3} \quad (6)$$

$$nf_{NH,LH,MH} = \int_{GF\_lim1}^{GF\_lim2} c(GF) dGF \quad (7)$$

where GF_lim1 and GF_lim2 represent, respectively, the lower and upper boundaries of the GF range for NH, LH or MH group, which can be determined by solving Eq. (5) with RH, dry diameter and corresponding boundaries of κ. The GF_{NH}, GF_{LH}, and GF_{MH} values are volume equivalent mean growth factors for the GF ranges of NH, LH and MH groups, respectively. The volume equivalent mean growth factor represents the equivalent growth factor if the absorbed water was equally distributed among all particles (Sjogren et al., 2008). The corresponding hygroscopicity parameters $\kappa_{NH,LH,MH}$ are determined by the $GF_{NH,LH,MH}$, the dry diameter D_0 and the calibrated relative humidity RH_{cal}, using Eq. (5). The ensemble mean growth factor is defined as a volume equivalent mean value of the GF-PDF over the whole GF range:

ACPD
11, 2991–3040, 2011

$GF_{mean} = \left(\int GF \cdot c(GF) dGF\right)^{1/3}$. The mean hygroscopicity parameters (κ_{mean}) are calculated from GF_{mean} and RH_{cal} using Eq. (5), which are basically equivalent to the mean value (1st-moment) of the κ-PDF (Probability Distribution Function of κ, $c(\kappa)$), and also equivalent to the average value of κ_{NH}, κ_{LH} and κ_{MH} weighted by their number fractions.

Note that both κ and ε_{AS} could be considered as proxies for an average or effective chemical composition of aerosol particles. To facilitate the comparison between the results of our study and previous studies, a simple approximation can be used to convert between each other:

$$\kappa = \kappa_{AS} \cdot \varepsilon_{AS} \approx 0.53 \varepsilon_{AS} \quad (8)$$

where κ_{AS} is the hygroscopicity parameter κ for ammonium sulphate, and its value is suggested to be 0.53 (growth factor derived) ~0.61 (CCN derived) by Petters and Kreidenweis (2007). Moreover, the concept of κ-PDF ($c(\kappa)$) is introduced in this study. Similar to the definition of GF-PDF, the κ-PDF represents the normalized distribution of κ. It can be converted from the GF-PDF using the following equation:

$$c(\kappa(GF)) = c(GF)[\partial\kappa(GF)/\partial GF]^{-1} \quad (9)$$

Here the κ(GF) is defined by Eq. (5). The differential of κ(GF) can be expressed as:

$$\partial\kappa(GF)/\partial GF = 3GF^2[\exp(A/GF)/S - 1] - (GF^3 - 1)[A/(SGF^2)\exp(A/GF)] \quad (10)$$

Where $A = (4\sigma_{s/a}M_w)/(RT\rho_w D_0)$. Given a series of paired GF and c(GF) values inverted from the TDMAinv algorithm, the corresponding κ(GF) and $c(\kappa(GF))$ values can be derived from Eqs. (5) and (9), respectively. Then the κ-PDF values at any κ, i.e., $c(\kappa)$ can be interpolated.

The state of mixing of aerosol particles can be implied from the GF-PDF or κ-PDF of the measurement scans. Each GF-PDF or κ-PDF represents a hygroscopicity distribution of particles with the same dry size. Since particles with different hygroscopicity generally represent distinct chemical compositions (or mixing ratio of chemical

ACPD
11, 2991–3040, 2011

compounds), the bimodal distribution of a GF-PDF or a κ-PDF generally indicates an external mixture. The size-resolved CCN activity can be also derived from the size-resolved κ-PDF. Recently, an article by Su et al. (2010) gave a detailed description of the hygroscopicity distribution concept, similar to the κ-PDF used here, for modelling aerosol mixing state with regard to hygroscopic growth and CCN activation. Sjogren et al. (2008) suggested using the standard deviation σ of the inverted GF-PDF (σ_{GF}) as a measure for the spread of growth factors, which was defined as:

$$\sigma_{GF} = \left(\frac{\int (GF - \overline{GF})^2 \cdot c(GF) dGF}{\int c(GF) dGF} \right)^{1/2} \quad (11)$$

where $\overline{GF} = \frac{\int GF \cdot c(GF) dGF}{\int c(GF) dGF}$. In this study, we calculated the standard deviation σ of κ-PDF (σ_κ) to estimate the spread of κ, thus represent the state of mixing in terms of hygroscopic growth, using the following equation:

$$\sigma_\kappa = \left(\frac{\int (\kappa - \overline{\kappa})^2 \cdot c(\kappa) d\kappa}{\int c(\kappa) d\kappa} \right)^{1/2} \quad (12)$$

where $\overline{\kappa} = \frac{\int \kappa \cdot c(\kappa) d\kappa}{\int c(\kappa) d\kappa}$. Any scan with large σ of κ-PDF value (e.g., >0.08) indicates that aerosol particles are highly externally mixed, while small σ of κ-PDF value (e.g., <0.08) indicates a state of low degree of external mixing or quasi-internal mixing. In this paper, the standard deviations of GF-PDF and κ-PDF for NH and MH modes are also presented, which can be calculated using Eqs. (11) and (12), respectively by integrating over corresponding ranges for GF or κ.

2.2.4 Correction of HH-TDMA data to set RHs

The HH-TDMA instrument was set at 90%, 95% and 98.5% RH. For 90% RH the fluctuations of RH were smaller than 1.5%, while for 95% and 98.5% RH the fluctuations

ACPD
11, 2991–3040, 2011

were normally within ±0.5%. Although the RH fluctuations were small, it is necessary to consider their effects on GF and GF-PDF, since the GF is very sensitive to RH at high RH range. In this study, all GF and GF-PDF were corrected to the set RHs unless marked otherwise.

For each measurement, the GF_{mean} and $GF_{NH,LH,MH}$ were corrected to their nominal value of RH (90%, 95% or 98.5%) using κ-Köhler model. The assumption of this correction is that κ is constant within the small RH ranges around the nominal RH values. Since our study shows that the RH-dependence of κ over RH range of 90% to 98.5% is small, we have reason to believe this assumption appropriate in this study. To conduct the RH correction for the GF, first the κ value was calculated by Eq. (5) using the measured GF and calibrated RH, and then the corrected GF at the nominally set RH was derived by solving Eq. (3) numerically. For GF-PDF, the RH correction is more complicated. Since the κ-Köhler model cannot be solved analytically for GF using RH and κ, the γ-model (Eq. 4 in Gysel et al., 2009) was chosen to calculate the RH correction for GF-PDF. The γ-model overcomes the computational difficulty of the κ-model in correcting GF-PDF, and comparison shows that the volume equivalent mean GF calculated by the GF-PDF corrected by the γ-model yields nearly the same results as the GF corrected by κ-Köhler model.

2.3 Regional meteorological model and aerosol box model

2.3.1 The WRF model

In this study, the Weather Research and Forecast Model (WRF, Skamarock et al., 2005) version 2.2 was used to generate the gridded meteorological fields. The simulation uses two nested domains with one-way nesting at resolutions of 18 km and 6 km, with 101 × 101 (1800 km × 1800 km) and 250 × 250 (1500 km × 1500 km) grid cells, respectively. There are 27 vertical levels using the eta coordinate in the simulations. The initial and boundary conditions were taken from the Global Forecast System (GFS, NCEP FNL, 1.0 × 1.0 degree) data at a 6-h resolution. The Yonsei University (YSU) boundary

ACPD
11, 2991–3040, 2011

layer scheme (Hong et al., 2006) and the 5-class microphysics scheme (WSM5) were used in the model. The simulated meteorological fields were available from 00:00 on 11 July to 00:00 on 15 August 2009 (UTC) for HaChi summer campaign. To better adapt the boundary conditions provided by NCEP data, these two campaigns were separated into several continuous 3-day short periods for WRF simulations. Each WRF run was initialized 12-h before the corresponding period, and the first 12-h data were used for modelling spin-up followed by the 3-day simulation period. The meteorological fields were output and stored every hour for analysis. In this paper, the simulated boundary layer (PBL) height was applied to initialize the PartMC-MOSAIC model (see Sect. 2.3.2). This high resolution meteorological field is also applied in other studies under HaChi project, such as back trajectory calculation (T. Göbel, personal communication, 2011).

2.3.2 The PartMC-MOSAIC model

The PartMC-MOSAIC recently developed by Riemer et al. (2009) is a stochastic particle-resolved aerosol box model, which explicitly resolves the composition of individual particles in a given population of different types of aerosol particles. The PartMC model uses a Monte-Carlo approach for simulating the coagulation process stochastically. Particle emissions and dilution with air representative of the regional, lower free tropospheric above the nocturnal boundary layer are also modelled in a stochastic manner. The PartMC was coupled with a new state-of-the-art aerosol chemistry module MOSAIC (Model for Simulating Aerosol Interactions and Chemistry, Zaveri et al., 2008), which simulates the gas and particle phase chemistries, particle phase thermodynamics, and dynamic gas-particle mass transfer in a deterministic manner. The coupled system predicts number, mass and full composition distributions. It treats all globally important aerosol species including sulphate, nitrate, chloride, carbonate, ammonium, sodium, calcium, other inorganic mass, primary organic aerosol (POA), secondary organic aerosol (SOA), and black carbon (BC). The hygroscopicity parameter κ for each aerosol particle is assumed to be the average of the κ values of the

ACPD
11, 2991–3040, 2011

constituent species weighted by their volume fractions. The assignment of individual κ values is taken from Riemer et al. (2010), assuming $\kappa = 0.65$ for all salts formed from the NH_4^+-SO_4^{2-}-NO^{3-} system, $\kappa = 0.1$ for SOA, $\kappa = 0.001$ for POA and $\kappa = 0$ for BC.

The simulated scenario represents a Lagrangian air parcel over a large megacity region. The simulation period is started at 18:00 h, 6 August and ended at 18:00 h 9 August 2009. The model was initialized 12-h before the simulation period for model adjustment. The mixing layer height was initialized based on the PBL height simulated by the WRF model and the temperature and water vapour mixing ratio were set based on the measurements. The initial gas phase concentrations and emission rates are the same as the idealized urban plume scenario described by Riemer et al. (2009), which assumed varied gas phase emissions throughout 06:00 to 18:00 according to a typical diurnal cycle found in a polluted urban area.

The initial aerosol distribution, which is representative of a regional average particle distribution, is tri-modal with an Aitken mode and two accumulation modes. The modal parameters of this distribution were adjusted to make the simulated aerosol concentration and distribution generally consistent with the observations using a TDMPS (Tandem Differential Mobility Particle Sizer) combined with an APS (Aerodynamic Particle Sizer). The initial aerosol was assumed to consist of $(NH_4)_2SO_4$, POA and BC, with mass fractions of about 60%, 35% and 5%, respectively. The composition of each particle was assumed to be identical, i.e., the initial particles were assumed to be internally mixed. The κ value of the initial aerosol is about 0.36. The mass concentration of the initial aerosol was about 40 $\mu g\,m^{-3}$, which is higher than that assumed in Riemer et al. (2009), representing the strong regional aerosol pollution in the North China Plain.

In Riemer et al. (2009) and Riemer et al. (2010), a constant particle emission was assumed during the day between 06:00 to 18:00 LT, and all emissions were switched off during the night. Three types of carbonaceous aerosols were considered in the emission: (1) meat cooking (100% POA), (2) diesel vehicle emissions (30% POA, 70% BC), and (3) gasoline vehicle emissions (80% POA, 20% BC). This assumption regarding emissions represents an urban plume scenario as described in Riemer et al. (2009).

ACPD
11, 2991–3040, 2011

Here, by contrast, we assume a particle emission with the same aerosol types, size distribution and composition as described by Riemer. However, particle emission was not switched off during the night (19:00–07:00 LT), but changed to 1/2 strength of that during 07:00–19:00 h LT instead. The emission rate during 07:00–19:00 LT was assumed to be the same as that used in Riemer et al. (2009). The assumption concerning particle emission in our study is basically consistent with the diurnal pattern of black carbon (BC) concentration during HaChi summer campaign observed by the MAAP (Ma et al., 2011), which generally shows a higher value during the night-time and lower value during day-time. This diurnal variation can be interpreted as a result of the diurnal variation of emission rate combined with the diurnal evolution of mixing height. A continued though lower emission of soot particles at night coupled with the shallow nocturnal mixing layer results in a higher concentration of BC during the night.

The PartMC-MOSAIC model is applied in this study to simulate the diurnal variations of aerosol hygroscopicity and mixing state for a 3-day scenario (from 6 to 9 August 2009). Comparison between the simulated results and the measurements of the HH-TDMA are presented in Sect. 4. The processes of coagulation, gas and particle phase chemistries and evolution of mixing layer are considered in the model, thus their effects on aerosol hygroscopicity and mixing state can be estimated.

3 Experiment results

The hygroscopic properties of aerosol particles with different dry diameters measured at the RH range between 90%–98.5% are analyzed and discussed here. The time series and diurnal variations of these properties are presented to show the different aerosol hygroscopic properties and different mixing states during daytime and night-time. A parameterisation of κ as function of dry diameter is provided and validated at four sizes within the interval 50–250 nm.

ACPD
11, 2991–3040, 2011

3.1 Distributions of GF and κ

Figure 2 shows the average GF-PDF as well as the corresponding average κ-PDF for particles with 50 nm, 100 nm, 200 nm and 250 nm dry diameters. The set values of RH are 90%, 95% and 98.5%, and the effect of instrumental RH fluctuation on GF-PDF has been corrected (see Sect. 2.2.4). Panels (a1)–(d1) show that the average growth distributions of 50 nm, 100 nm, 200 nm and 250 nm particles are uniformly bimodal. A dominate more-hygroscopic mode and a smaller but distinct, nearly-hydrophobic mode can be observed for each averaged GF-PDF. The peaks of MH modes in GF-PDF shift significantly from about 1.4–1.6 to 2.1–2.8 (depend on different dry diameters) as the RH increases from 90% to 98.5%, whereas the peaks of NH modes only shift very slightly from about 1.1 to a value of about 1.2; the spread of both modes becomes wider as the RH increases. For the average GF-PDFs with same RH, the peak of MH mode shifts to larger values when the dry diameter increases from 50 nm to 250 nm, indicating that the hygroscopic particles with larger dry diameters generally have greater growth factors compared to the smaller hygroscopic particles. Panels (a2)–(d2) show that the measurements at 90%, 95% and 98.5% RH generally achieve similar average distributions of hygroscopicity parameter κ, indicating that the hygroscopic growths of monodisperse particles measured at different RHs yield consistent results via κ-Köhler model. Similar to the GF-PDF, two distinct modes can be seen for each κ-PDF. The classification of the three different hygroscopic groups described in Sect. 2.2.3 is shown to be appropriate (see Fig. 2a2–d2), since this classification adequately captures the NH mode and the MH mode for most scans at all RHs and for all dry diameters. The transition regions between the two distinct modes are defined as the LH group, which is overall less important in this study though the LH group has a larger fractional contribution to the PDF at smaller sizes. The average κ-PDF represents the probability of the occurrence of particles with different hygroscopicity. It means that not only the mixing state but also the temporal variability of hygroscopicity contributes to the spread of κ-PDF. The aerosol mixing state will be discussed in the following sections.

ACPD
11, 2991–3040, 2011

It is noted that the κ value for the peaks of the NH mode in the κ-PDFs decreases slightly as the RH increases. However, considering the inversion resolution (0.075 in GF for 90% RH and 0.125 for 98.5% RH) and the instrumental uncertainty limits, it is not easy to resolve the detailed hygroscopicity distributions for the nearly-hydrophobic particles, especially at 90% RH. The slight shifts of NH mode in κ-PDFs do not necessarily indicate that the hygroscopicity of the NH group particles has a RH-dependent behaviour. As the RH increases from 90% to 98.5%, the peak of NH in GF-PDF remains at GF = 1.1, but the spread becomes wider at the same time. We calculated the number fractions of particles with GF<1.2, and the results show that these values decrease significantly as the RH increase, as presented in Table 1. Taking particles with 100 nm dry size as an example, the number fractions of GF < 1.2 at 90%, 95% and 98.5% are 0.16 ± 0.10, 0.14 ± 0.09 and 0.09 ± 0.08, respectively. By contrast, the number fraction of particles with $\kappa < 0.1$ (NH group) at three RHs are 0.16 ± 0.10, 0.18 ± 0.11 and 0.15 ± 0.11. This result indicates that some particles in the NH group are internally mixed with small amounts of soluble materials (e.g., sulphate, nitrate, etc), or SOA with some sparingly soluble materials; thus, an observable growth behaviour appears at very high RH (>95%). This slight change in hygroscopic growth behaviour cannot be resolved without taking advantage of the high RH hygroscopic measurement. In other words, hygroscopicity measurements at high RH provide detailed information about the distributions of hygroscopicity.

The statistics of the HH-TDMA measurements are summarized in Table 1. The particles are classified into the different hygroscopic groups, as described in Sect. 2.2.3. The mean GF, mean κ, mean nf and spread of GF and κ for the NH and MH groups for the whole HaChi summer campaign are presented in Table 1. These parameters, calculated as ensemble mean for all groups, are presented as well. Significant hygroscopic diameter growth behaviours were observed at RH ranges from 90%–98.5% for MH particles with 50 nm, 100 nm, 200 nm and 250 nm dry diameters. Taking particles with 100 nm dry size as an example, the mean GF for the MH group at 90%, 95% and 98.5 RH are 1.54, 1.81 and 2.45, respectively; whereas the mean GF for NH group

ACPD
11, 2991–3040, 2011

particles increases slightly from 1.08 at 90% RH to 1.24 at 98.5% RH. No significant variations of mean κ or nf were observed at different RHs. Both mean GF and mean κ for all groups and for MH groups increase as a function of particle dry diameter. The mean κ of all groups increases from around 0.25 to 0.34 as the dry diameter increases from 50 nm to 250 nm, indicating that, besides the Kelvin effect, the size dependence of GF is due to the variation of hygroscopicity parameter κ, and hence also due to the difference of chemical composition for particles with different size. For NH group particles, the mean κ decreases from about 0.05 for 50 nm particles to about 0.02 for 250 nm particles.

3.2 Time series, meteorology and diurnal variation

The meteorological parameters, e.g., wind direction (WD), wind speed (WS), temperature (T) and relative humidity (RH) were continuously measured at Wuqing meteorological station by instruments which were beside the containers with the aerosol instruments. The time series of meteorological parameters are presented in Fig. 3, panels (a) and (b). The ambient T and RH both show pronounced diurnal variation with high temperature and low RH during the day and the opposite during the night. For particles with 100 nm dry diameter, the time series of hygroscopicity parameters for all groups (κ_{mean}), MH group (κ_{MH}) and NH group (κ_{NH}) are shown in panels (c)–(e), and the number fraction of MH group (nf_{MH}) and NH group (nf_{NH}) are illustrated in panels (f)–(g), respectively. Panels (c)–(g) demonstrate that the hygroscopicity parameters and number fractions measured at 90%, 95% and 98.5% RH generally yield consistent results, indicating that the RH-dependence of aerosol hygroscopicity κ is not important in the RH range between 90%–98.5% in this study. Figure 4 depicts the results of autocorrelation analysis for meteorological parameters (panel a) and for κ_{mean}, κ_{MH} and nf_{NH} of 100 nm dry diameter particles measured at three RHs (panel b). The correlation coefficient of ambient T and ambient RH show sinusoidal variations, with high values of 0.5–0.6 when $\Delta t = 24$, 48 and 72 h, demonstrating the pronounced diurnal variations of these variables. These results are consistent with those depicted

ACPD
11, 2991–3040, 2011

in Fig. 3a and b. Similarly, autocorrelation analysis shows that the diurnal variation of nf_{NH} is pronounced, and that of κ_{mean} is relatively weaker, but it is still significant. The diurnal variation for the κ_{MH} was found to be less obvious (see Fig. 4b). The time series and autocorrelation analysis indicate that the fraction of NH particles, e.g., freshly emitted soot, varies greatly during a day while the hygroscopicity of MH group particles is relatively stable during the measurement period. The variation of hygroscopicity of all groups is largely due to the diurnal variation of number fraction of NH group particles.

The average diurnal variations of κ_{mean}, κ_{MH} and nf_{NH} of 50 nm, 100 nm, 200 nm and 250 nm dry diameters during HaChi summer campaign are presented in Fig. 5a–c. These parameters generally show different characteristics between daytime and nighttime measurements. An apparent feature of the diurnal pattern is that the nf_{NH} of all dry diameters changes significantly with time of a day (see Fig. 5c). The average nf_{NH} between 18:00 to 09:00 (night-time) is about 20%, while between 09:00 to 18:00 (day-time) it is about 8%. A significant decrease and rapid increase of nf_{NH} were often observed at 08:00 to 10:00 and at around 18:00, respectively. Figure 5a shows that the average κ_{mean} for 100 nm, 200 nm and 250 nm particles increases slightly during the day, while the average κ_{mean} for 50 nm increases significantly, representing that the hygroscopicity of aerosol particles with 50 to 250 nm dry diameters is enhanced during the day due to the decrease of the fraction of NH particles. The differences of κ_{MH} for particles with different dry diameters are smaller during the day than during the night (see Fig. 5b), indicating that during the day the chemical composition is more evenly distributed across dry diameter. Figure 5d indicates that the spread of κ-PDF, which basically represents the dispersion of chemical composition (in terms of the hygroscopic growth) among particles with the same dry diameters, decreases during the day.

The diurnal patterns of the parameters mentioned above reflect the variation of aerosol mixing states. The high number fraction of NH particles during the night indicates that the freshly emitted hydrophobic particles, (e.g., fresh soot or primary organic aerosol, see Petters et al., 2006, and Zhang et al., 2008) have accumulated in

ACPD
11, 2991–3040, 2011

the surface layer, apparently externally mixed with the hygroscopic particles. During the day, the fraction of NH mode, nf_{NH}, is smaller (see Fig. 5c), indicating that aged aerosol was dominant in the atmosphere near the surface. Figure 5a, b and d shows clearly that differences in hygroscopicity, κ, among particles are less apparent during the day, indicating that the extent of external mixing is lower in the daytime compared to that at night. Similar results regarding the diurnal variations of aerosol mixing state were reported by Moffet and Prather (2009) and Lance (2007). Their measurements were also made in a megacity area (Mexico City) with aerosol mass spectrometer (AMS) and cloud condensation counter (CCNC) instruments. We will present a meteorological and aerosol modelling study in Sect. 4 to interpret the observed diurnal variation of aerosol mixing state.

3.3 Hygroscopic growth at high humidity

During the HaChi summer campaign, the HH-TDMA was set to measure at RH of 90%, 95% and 98.5% for particles with 50 nm, 100 nm, 200 nm and 250 nm dry diameters, providing detailed information about hygroscopic growth at RH above 90%. A mobile version of Leipzig Aerosol Cloud Interaction Simulator (LACIS-mobile; Stratmann et al., 2004; Wex et al., 2006) instrument was installed in the same measurement container and operated in parallel with the HH-TDMA. During the campaign, LACIS-mobile was set to measure the aerosol hygroscopic growth factor over the RH range between 97.9% and 99.5% for particles with 200 nm and 250 nm dry diameter. The results of LACIS-mobile are also presented here as a reference (see the circles in Fig. 6c1, d1). Since LACIS-mobile can only measure particles which have grown to a larger size, only the GF of hygroscopic particles can be shown here.

Figure 6a1–d1 shows the hygroscopic growths of aerosol particles with 50 nm, 100 nm, 200 nm and 250 nm dry diameters, respectively. The squares and crosses represent the average growth factors of MH group and NH group measured by the HH-TDMA, respectively (corrected to the nominal RHs), and the error bars denote the standard deviations; red and blue colours represent measurements during the day

ACPD
11, 2991–3040, 2011

(09:00–18:00 LT) and during the night (18:00–09:00 LT), respectively. The fitted curves are κ-Köhler curves using the averaged κ measured at all RHs. The reference curves (green solid curves) are calculated Köhler curves for ammonium sulphate particles, using the scheme from Low (1969) and Young and Warren (1992). It can be seen that the growth curves can be well described with the single-parameter (κ) Köhler model given in Eq. (3). Over time, remarkably consistent hygroscopic growths were observed for hygroscopic group particles with all dry diameters, i.e. the variance was low. Compared to the hygroscopic growth factors of pure ammonium sulphate particles, those of MH group particles with 50 nm and 100 nm dry diameters reveal relatively lower values (see Fig. 6a1 and b1), indicating that these particles are quasi-internal mixtures of both inorganic compounds (e.g., sulphate, nitrate and sodium chloride, with strong hygroscopicity) with organic compounds (normally slightly hygroscopic or hydrophobic), or an insoluble core (e.g., soot or dust) with inorganic coating. By comparison, MH group particles with 200 nm and 250 nm dry diameters demonstrate larger hygroscopic growth factors (see Fig. 6c1 and d1). The diameters are enhanced at high RH, by a factor of about 1.6 at 90% and about 4 at 99.5% RH. These pronounced growths in diameter imply dramatic enhancement in aerosol scattering with a correspondingly large change in other aerosol optical properties at high RHs. The hygroscopic growths of 200 nm and 250 nm MH group particles are only slightly lower than those of the pure ammonium sulphate particles, indicating that these particles contain large fractions of inorganic compounds. The predicted growth factors of MH group particles using κ derived from the HH-TDMA are highly consistent with the LACIS results at RH < 98.5% (see Fig. 6c1 and d1), but are slightly lower than that measured by LACIS (e.g. predicted GF of 3.7 cf. LACIS GF of 3.9 at 200 nm and 99.5% RH, nighttime). This slight difference indicates a possible RH-dependence of κ, which could be enhanced at very high RH (>98.5%). The error bars of GF_{MH} measured by the HH-TDMA are generally small, indicating that the temporal variations of GF_{MH} at the same RH (due to the variations of hygroscopicity) are less significant than the variations of GF_{MH} due to the change of RH. Both HH-TDMA and LACIS-mobile show that the hygroscopicity of MH

ACPD
11, 2991–3040, 2011

group particles with 200 nm and 250 nm dry diameters during the day is about 9% lower in terms of κ than that during the night.

The diameter enhancements for the NH group particles at high RH are less pronounced compared to those for the MH group particles. The GF_{NH} values are generally lower than 1.2–1.3 during the night at RH < 98.5%. During the day, the average GF_{NH} values are slightly higher and the standard deviations (which show the temporal variations) are larger than those during the night. Figure 6a2–d2 shows the average number fractions of three hygroscopic groups during daytime and nighttime, respectively.

3.4 Parameterization of HH-TDMA data

In Sect. 2.2.3 we introduced a method to classify particles into different groups using the hygroscopicity parameter κ. The κ as well the GF values are presented in Table 1 to describe the hygroscopic growth of aerosol particles. In Sect. 3.2, we discussed that measurements of GF and nf at different RHs are internally consistent through the parameter κ, within the RH range between 90% and 98.5%. In Sect. 3.3, κ was chosen as the more desirable way to describe the hygroscopic growth of aerosol particles. To further facilitate the use of HH-TDMA data, κ can be parameterized as a function of dry diameter, D_0, using the equation (Rissler et al., 2006):

$$\kappa(D_0) = B\log(D_0) + CD_0 + D \quad (13)$$

where B, C and D are fitted parameters. In Rissler et al. (2006), an equation similar to Eq. (13) as presented here was used to parameterize the size-dependent variation of A, where A is identical to κ in principle, if the Kelvin term in Eq. (3) is neglected. Similarly, the nf is also parameterized as a function using the same equation as Eq. (13), by replacing $\kappa(D_0)$ with $\mathrm{nf}(D_0)$. Examples for the parameterizations are presented in Fig. 7. The value of κ for the MH group particles measured during the night increases significantly with particle dry diameter, suggesting an increasing fraction of soluble components. However, the κ_{MH} is significantly less than the κ of pure ammonium sulphate particles (green lines). During the day, the κ_{MH} increases slightly for diameters

ACPD
11, 2991–3040, 2011

greater than 100 nm, indicating that the variation of soluble fraction with diameter is less pronounced than that during the night. For 50 nm MH particles, daytime measurements show stronger hygroscopicity, which suggest that the Aitken mode particles may have different sources during the day and during the night. In contrast to the MH group described above, the κ of NH group particles decreases slightly as a function a dry diameter, for both day and night measurements.

In this study, κ and nf for MH group, NH group and ensemble mean for all groups during the day, during the night and during the whole period have been fitted empirically as described above. The values of the parameters in Eq. (13) are summarized in Table 2. The parameterized GFs can be derived by solving Eq. (3) using κ values calculated from Eq. (13) combined with parameters in Table 2. A lookup table was made for GF values as a function of dry diameter and RH. The result is illustrated in Fig. 8 panels (a)–(c), which show the parameterized mean GF of all groups for daytime, night-time and whole period measurements, respectively. GF values which are represented by the colour of the contour lines can be read directly from the figure. Similar lookup tables or contour figures can also be made for each hygroscopic group separately, using the data in Table 2. To validate our parameterization for GF, Fig. 8d presents a comparison between the parameterized GF and the measured GF. The comparison result shows that, in most cases our parameterizations adequately capture the variations of GF and nf as functions of dry diameter and RH (90%–98.5%). For the GF of NH group during the night at 98.5% RH, the parameterized GF deviates slightly from the measured values. Since the parameterizations are based on the measured size range 50–250 nm, we do not recommend extrapolating Eq. (13) to particles larger than 250 nm or smaller than 50 nm. It is worth to note that Meier et al. (2009) and Eichler et al. (2008) observed a decreasing trend in GF for particles larger than 300 nm, based on the measurements conducted in Beijing (North China Plain) and Xinken (Pearl River Delta in South-Eastern China), respectively.

ACPD
11, 2991–3040, 2011

4 Diurnal variations of aerosol hygroscopicity and mixing state: a case study

4.1 Description of meteorological situation

To better understand the chemical and meteorological processes dominating the diurnal variation of aerosol hygroscopicity and mixing state, a state-of-the-art, stochastic, particle-resolved aerosol model PartMC-MOSAIC was applied to simulate the aerosol hygroscopicity and mixing state (see Sect. 2.3.2 for the description of the model). A 3-day period from 6 August 18:00 LT to 9 August 2009, 18:00 LT was selected for the simulations. Influenced by the slow-moving typhoon "Morakot" near Taiwan about 2000 km south from the site, the synoptic situation of Wuqing during this period was relatively constant, with $<3\,m\,s^{-1}$ east wind dominating this area most of the time (see Fig. 3a, where the selected period is marked). The weather was cloud-free, without precipitation. Under this meteorological situation, the pollution in the surface layer was dominated by the local or regional emissions. Thus, the meteorological situation was well suited for the investigation of the diurnal variations of aerosol properties via PartMC-MOSAIC.

4.2 Description of the simulated cases

There are several plausible mechanisms to explain the diurnal behaviour of aerosol mixing state, all of which are likely consistent with the measurements described in Sect. 3.2 (Petters et al., 2006; Riemer et al., 2009; Moffet and Prather, 2009; Lance, 2007; Rissler et al., 2006): (1) condensation of secondary organic and inorganic species onto the hydrophobic particles; (2) photochemical oxidation on the surface or in the interior of hydrophobic particles; (3) coagulation of hydrophobic particles with more hygroscopic background particles; (4) the downward mixing by entrainment of more aged, hygroscopic particles from aloft due to the break-up of the nocturnal inversion layer.

ACPD
11, 2991–3040, 2011

The PartMC-MOSAIC model consists of two parts: the PartMC model (Riemer et al., 2009) deals with the coagulation process, particle emissions and dilution in a stochastic manner; while the aerosol chemistry module MOSAIC (Zaveri et al., 2008) simulates the gas and particle phase chemistries, particle phase thermodynamics, and dynamic gas-particle mass transfer deterministically. The effects of these mechanisms on aerosol hygroscopicity and mixing state, can be isolated by designing different model simulation cases. We initially assumed 2×10^4 particles in the air parcel for the stochastic simulations. Table 3 shows the experimental design for the mechanism settings used in this study. For case 1, coagulation was switched off in PartMC model, and the MOSAIC chemistry module was disabled in the simulation. Different emission rates of anthropogenic carbonaceous aerosols were set for daytime and nighttime (see Sect. 2.3.2). A variable mixing height (see Fig. 9a) was adapted from the simulation of WRF model (see Sects. 2.3.1 and 2.3.2). Thus, in this case, with condensation, photochemical oxidation and coagulation processes disabled, increases of mixing height and entrainment of air from aloft with a lower concentration of internally mixed aerosols during the morning, resulted in the dilution of surface aerosol concentrations and the change of the overall aerosol mixing state. For case 2, the coagulation process was switched on and other settings were kept the same as case 1. For case 3, the PartMC model was coupled with the gas-particle chemistry module MOSAIC and others were the same as case 2, thus all mechanisms mentioned above were considered in the case-3 simulation. For case 4, the mixing height was fixed to 1000 m (see Fig. 9a) base on case 3. Thus, the entrainment of aerosol from aloft in the morning was disabled while the evolution of aerosol properties in the air parcel were driven by the aging processes e.g., coagulation, condensation of secondary organic and inorganic species, and photochemical oxidation.

4.3 Simulated and measured aerosol properties

The comparison of modelled and measured aerosol properties is shown in the lower two panels of Fig. 9. The magnitude and diurnal pattern of the simulated concentrations

ACPD
11, 2991–3040, 2011

and hygroscopicity of total aerosol and black carbon are generally consistent with the measurements of nf_{NH} and κ_{mean}. The modelled external mixed BC and POA (with $\kappa < 0.1$) are considered to be a proxy for NH particles and are compared to the modelled total number concentration to yield a modelled nf. The volume-weighted average κ for all modelled components is compared to the measured κ_{mean}. Both the simulation (case 3 in which all mechanisms were included) and measurements show that the concentrations of both total aerosol and black carbon are lower during the day than during the night, due to the dilution in the morning when the mixing height increases. More information about the measured diurnal variations of aerosol mass concentration and BC mass concentration can be found in Ma et al. (2011).

Figure 9b and c shows that the diurnal variations of nf_{NH} and κ_{mean} for 100 nm particles measured by the HH-TDMA are very pronounced during our simulation period. The nf_{NH} of 100 nm particles is generally low in the afternoon (about 0 to 10%), indicating that most of the aerosol particles are more hygroscopic; while the nf_{NH} increases rapidly after 18:00 LT when the PBL collapses and the HH-TDMA measurements show clear bi-modal distributions of GF-PDF and κ-PDF, which indicate that the aerosol particles are externally mixed (see Fig. 9b). The mean κ of all groups shows the inverse diurnal pattern. The κ_{mean} for 100 nm dry diameter particles is about 0.2 during the night, and increases rapidly in the morning to about 0.3. The diurnal variations of nf_{NH} and κ_{mean} of 50 nm, 200 nm and 250 nm particles are similar to those of 100 nm particles described above. The diurnal patterns of nf_{NH} and κ_{mean} of particles with 100 nm dry diameter can be well depicted by the PartMC-MOSAIC simulations of case 1, 2 and 3, in which the process of aerosols entrainment from aloft in the morning is included. In contrast, simulation of case 4 has failed to capture these diurnal variations. In case 4, aging processes such as coagulation, condensation and photochemical aging are included, but we assumed a fixed mixing height to prevent the dilution and entrainment of background aerosols in the morning when the actual mixing height is increasing. These results indicate that the entrainment of background aged particles in the morning is decisive in explaining the diurnal cycle of aerosol hygroscopicity and mixing state.

ACPD
11, 2991–3040, 2011

In the morning (~07:00 LT), the increasing mixing height brings a downward entrainment of more aged and hygroscopic particles from aloft leading to the decrease of nf_{NH} and increase of κ_{mean}; while in the evening (after 18:00 LT) the shallow nocturnal stable layer combined with the local emission of black carbon aerosols (e.g., soot emitted from diesel truck engines during the night) explain the rapid increase of hydrophobic particle fraction and the decrease of the mean hygroscopicity. A similar boundary layer mechanism was suggested by Rissler et al. (2006) to explain the diurnal pattern of number concentration, size distribution and hygroscopic properties for biomass burning aerosols in Amazonia. In this study, we use a particle-resolved aerosol model to estimate the effects of downward mixing of more aged aerosol in the morning hour and confirm that this mechanism is a plausible explanation for the diurnal pattern of aerosol hygroscopicity and mixing state. We should also notice that in the simulations we assume the initial aerosols are internal mixture of sulphate, OC and BC since the these aerosols have longer time for aging processes than the aerosols in the surface layer near emissions and the cloud processing may also accelerate the aging of lofted aerosol particles. Although we consider that this assumption is reasonable, more direct three-dimension measurements of aerosol mixing state (e.g., Pratt and Prather, 2010) could be valuable for our scientific understanding.

Comparisons among the results of case 1, 2 and 3 indicate as expected that the aging processes such as coagulation, condensation of organic/inorganic species and photochemical aging also contribute to the variations of the aerosol hygroscopicity and mixing state. Case 2 (with coagulation) demonstrates slightly lower hygroscopicity for 100 nm particles compared with case 1. This could be interpreted as the transformation via coagulation of the smaller particles (~50 nm) which contain large number fraction of fresh soot into larger (~100 nm) less-hygroscopic particles, resulting in the decrease of mean hygroscopicity measured for 100 nm particles. Comparison between case 3 and case 2 shows that the condensation and photochemical aging processes could significantly increase the mean hygroscopicity for 100 nm particles. The chemical aging effects are more pronounced in the afternoon (12:00–18:00 LT) due to the formation of

ACPD
11, 2991–3040, 2011

secondary species. However, the chemical aging and coagulation aging are insufficient in explaining the pronounced diurnal variations of mean hygroscopicity and mixing state observed in this study (see Fig. 9b and c).

5 Conclusions

For the first time in this geographical and pollution source region of the North China Plain, we employed the HH-TDMA to investigate the atmospheric aerosol and provide a detailed description of its hygroscopic properties and mixing state at high RH between 90 and 98.5%. The measurements were conducted from 17 July 2009 to 12 August 2009. These in-situ field measurements of atmospheric aerosol are unique with respect to their high RH range and especially of importance to better understand the widespread anthropogenic haze over the North China Plain.

The average GFs of particles with 50–250 nm dry diameters measured at 90%, 95% and 98.5% RHs are 1.39–1.57, 1.57–1.89 and 1.97–2.70, respectively. The average GF measured at the same RH generally increased as a function of dry diameter. The corresponding average hygroscopicity parameter κ was also determined, ranging from 0.25 to 0.34 for 50 to 250 nm particles. The average GF-PDF reveals a bi-modal distribution with two distinct peaks and an intermediate transition region. To facilitate the comparison and interpretation of HH-TDMA data measured at different RHs and for different particle size, the inverted GF-PDFs were classified into nearly-hydrophobic ($\kappa < 0.1$, first peak), less-hygroscopic ($\kappa = 0.1$ to 0.2, transition) and more-hygroscopic ($\kappa > 0.2$, second peak) groups. Based on this classification of hygroscopic groups using the criteria of κ, the hygroscopic properties measured at different RHs yielded consistent results in terms of κ, indicating that the κ-theory is adequate in describing the hygroscopic growth of atmospheric aerosol at a RH range between 90%–98.5%. Detailed analysis regarding RH-dependence of κ at high RH (90% to 99.5%) will be presented by Mildenberger et al. (2011). Particles of the more-hygroscopic group are generally dominant for the measured size range of 50 to 250 nm, and the average

ACPD
11, 2991–3040, 2011

fraction of the more-hygroscopic group is slightly higher for larger particles, ranging from 68% to 85% for 50 to 250 nm particles. The hygroscopic growth of the more-hygroscopic group was relatively stable during the period, with average κ values of 0.30 to 0.39 for 50 to 250 nm particles. Although the more-hygroscopic atmospheric aerosols reveal lower hygroscopicity than pure ammonium sulphate (with $\kappa = \sim 0.5$ to 0.6), these particles experienced large hygroscopic growth at high RH (>90%), their size being increased by $2.1 \sim 2.8$ fold at 98.5% RH and about 4-fold at 99.5% RH (from LACIS measurements) as compared to dry particles. These hygroscopic growth behaviours also reveal an immense potential of light scattering enhancement at high humidity and the potential for being highly effective cloud condensation nuclei.

The variation of the mean hygroscopicity of all groups is mostly due to the pronounced diurnal pattern for the number fractions of different groups. The average number fraction of nearly-hydrophobic particles during day-time (09:00–18:00 LT) is about 8%, while during the night the fraction reaches about 20%. An inverse diurnal pattern of the number fraction of more-hygroscopic particles was correspondingly observed. This variation in number fraction also indicates a change in aerosol mixing state. Based on the spread of κ-PDF, most of the scans measured during the night demonstrated distinctly external mixing states, while during the day the degree of external mixing was less. A case study for a three day period with stable meteorological conditions was conducted to investigate the diurnal pattern of hygroscopicity and mixing state, using a particle-resolved aerosol model PartMC-MOSAIC. In the case study, the high fraction of nearly-hydrophobic particles during the night was well explained by the shallow nocturnal layer combined with fresh soot emissions from traffic while the rapid decrease in the number fraction of nearly-hydrophobic particles and the corresponding increase in the mean κ in the morning hours are mostly due to the entrainment of aged and hygroscopic particles from the residual layer aloft as the stable layer breaks down. The condensation, photochemical aging and coagulation processes are also included in the simulations and they could contribute to the variation of aerosol hygroscopicity and mixing state as expected. However, these aging processes alone

ACPD
11, 2991–3040, 2011

were evaluated to be insufficient in magnitude or rate to interpret the observed diurnal pattern of hygroscopicity and mixing state in terms of hygroscopic growth.

Acknowledgements. The authors thank M. Gysel for the use of the TDMA inversion algorithm (TDMAinv). The authors acknowledge N. Riemer, M. West and R. A. Zaveri for their provision and guidance of the PartMC-MOSAIC model. The invaluable comments from D. S. Covert, D. Lamb, J. P. Chan and R. Shaw are also gratefully acknowledged. This work is supported by the National Natural Science Foundation of China (NSFC) under Grant No. 40875001, the German Science Foundation under grant DFG WI 1449/14-1 and the 973 Program (2011CB403402).

References

Albrecht, B. A.: Aerosols, cloud microphysics, and fractional cloudiness, Science, 245, 1227–1230, 1989.

Charlson, R. J., Schwartz, S. E., Hales, J. M., Cess, R. D., Coakley Jr., J. A., Hansen, J. E., and Hofmann, D. J.: Climate forcing by anthropogenic aerosols, Science, 255, 423–430, doi:10.1126/science.255.5043.423, 1992.

Cheng, Y. F., Wiedensohler, A., Eichler, H., Heintzenberg, J., Tesche, M., Ansmann, A., Wendisch, M., Su, H., Althausen, D., Herrmann, H., Gnauk, T., Brüggemann, E., Hu, M., and Zhang, Y. H.: Relative humidity dependence of aerosol optical properties and direct radiative forcing in the surface boundary layer at Xinken in Pearl River Delta of China: An observation based numerical study, Atmos. Environ., 42, 6373–6397, 2008.

Deng, Z. Z., Zhao, C. S., Zhang, Q., Huang, M. Y., and Ma, X. C.: Statistical analysis of microphysical properties and the parameterization of effective radius of warm clouds in Beijing area, Atmos. Res., 93, 888–896, 2009.

Eichler, H., Cheng, Y. F., Birmili, W., Nowak, A., Wiedensohler, A., Brüggemann, E., Gnauk, T., Herrmann, H., Althausen, D., Ansmann, A., Engelmann, R., Tesche, M., Wendisch, M., Zhang, Y. H., Hu, M., Liu, S., and Zeng, L. M.: Hygroscopic properties and extinction of aerosol particles at ambient relative humidity in south-eastern China, Atmos. Environ., 42, 6321–6334, 2008.

Gysel, M., Crosier, J., Topping, D. O., Whitehead, J. D., Bower, K. N., Cubison, M. J., Williams, P. I., Flynn, M. J., McFiggans, G. B., and Coe, H.: Closure study between chemical compo-

ACPD
11, 2991–3040, 2011

sition and hygroscopic growth of aerosol particles during TORCH2, Atmos. Chem. Phys., 7, 6131–6144, doi:10.5194/acp-7-6131-2007, 2007.
Gysel, M., McFiggans, G. B., and Coe, H.: Inversion of tandem differential mobility analyzer (TDMA) measurements, J. Aerosol Sci., 40, 134–151, doi:10.1016/j.jaerosci.2008.07.013 2009.
Hennig, T., Massling, A., Brechtel, F. J., and Wiedensohler, A.: A tandem DMA for highly temperature-stabilized hygroscopic particle growth measurements between 90% and 98% relative humidity, J. Aerosol Sci., 36, 1210–1223, doi:10.1016/j.jaerosci.2005.01.005, 2005.
Hong, S.-Y., Noh, Y., and Dudhia, J.: A new vertical diffusion package with an explicit treatment of entrainment processes, Mon. Weather Rev., 134, 2318–2341, doi:10.1175/MWR3199.1, 2006.
Jacobson, M. Z.: Strong radiative heating due to the mixing state of black carbon in atmospheric aerosols, Nature, 409, 695–697, 2001.
Köhler, H.: The nucleus in and the growth of hygroscopic droplet, Trans. Faraday Soc., 32, 1152–1161, doi:10.1039/TF9363201152, 1936.
Lance, S.: Quantifying compositional impacts of ambient aerosol on cloud droplet formation, PhD thesis, School of Earth and Atmospheric Sciences, Georgia Institute of Technology, Atlanta, 166 pp., 2007.
Leitte, A. M., Schlink, U., Herbarth, O., Wiedensohler, A., Pan, X.-C., Hu, M., Richter, M., Wehner, B., Tuch, T., Wu, Z., Yang, M., Liu, L., Breitner, S., Cyrys, J., Peters, A., Wichmann, H. E., and Franck, U.: Size segregated particle number concentrations and respiratory emergency room visits in Beijing, China, Environ. Health Perspect., doi:10.1289/ehp.1002203, in press, 2011.
Liu, P. F., Zhao, C. S., Zhang, Q., Deng, Z. Z., Huang, M. Y., Ma, X. C., and Tie, X. X.: Aircraft study of aerosol vertical distributions over Beijing and their optical properties, Tellus B, 61, 756–767, 2009.
Low, R. D. H.: A generalized equation for the solution effect in droplet growth, J. Atmos. Sci., 26, 608–611, 1969.
Ma, N., Zhao, C. S., Nowak, A., Müller, T., Cheng, Y. F., Deng, Z. Z., Liu, P. F., Xu, W. Y., Ran, L., Yan, P., Göbel, T., Hallbauer, E., Mildenberger, K., Henning, S., Yu, J., Liang, W. D., Cheng L. L., Zhou, X. J., Stratmann, F., and Wiedensohler, A.: Aerosol Optical Properties in the North China Plain during HaChi Campaign: an In-situ Optical Closure Study, Atmos. Chem. Phys. Discuss., in preparation, 2011.

ACPD
11, 2991–3040, 2011

Massling, A., Stock, M., Wehner, B., Wu, Z. J., Hu, M., Brüggemann, E., Gnauk, T., Herrmann, H., and Wiedensohler, A.: Size segregated water uptake of the urban submicrometer aerosol in Beijing, Atmos. Environ., 43, 1578–1589, 2009.

Menon, S., Hansen, J., Nazarenko, L., and Luo, Y.: Climate effects of black carbon aerosols in china and india, Science, 297, 2250–2253, doi:10.1126/science.1075159, 2002.

Meier, J., Wehner, B., Massling, A., Birmili, W., Nowak, A., Gnauk, T., Brüggemann, E., Herrmann, H., Min, H., and Wiedensohler, A.: Hygroscopic growth of urban aerosol particles in Beijing (China) during wintertime: a comparison of three experimental methods, Atmos. Chem. Phys., 9, 6865–6880, doi:10.5194/acp-9-6865-2009, 2009.

Mildenberger, K., Henning, S., Nowak, A., Sommerhage, E., Schäfer, M., Hallbauer, E., Göbel, T., Nekat, B., van Pinxteren, D., Deng, Z. Z., Liu, P. F., Ma, N., Zhao, C. S., Herrmann, H., Wiedensohler, A., and Stratmann, F.: A Hygroscopicity Closure Study for Atmospheric Aerosol Particles in the North China Plain, in preparation, 2011.

Moffet, R. C. and Prather, K. A.: In-situ measurements of the mixing state and optical properties of soot with implications for radiative forcing estimates, Proc. Natl. Acad. Sci., 106, 11872–11877, doi:10.1073/pnas.0900040106, 2009.

Oshima, N., Koike, M., Zhang, Y., Kondo, Y., Moteki, N., Takegawa, N., and Miyazaki, Y.: Aging of black carbon in outflow from anthropogenic sources using a mixing state resolved model: Model development and evaluation, J. Geophys. Res., 114, D06210, doi:10.1029/2008jd010680, 2009.

Petters, M. D. and Kreidenweis, S. M.: A single parameter representation of hygroscopic growth and cloud condensation nucleus activity, Atmos. Chem. Phys., 7, 1961–1971, doi:10.5194/acp-7-1961-2007, 2007.

Petters, M. D., Prenni, A. J., Kreidenweis, S. M., DeMott, P. J., Matsunaga, A., Lim, Y. B., and Ziemann, P. J.: Chemical aging and the hydrophobic-to-hydrophilic conversion of carbonaceous aerosol, Geophys. Res. Lett., 33, L24806, doi:10.1029/2006GL027249, 2006.

Petters, M. D., Wex, H., Carrico, C. M., Hallbauer, E., Massling, A., McMeeking, G. R., Poulain, L., Wu, Z., Kreidenweis, S. M., and Stratmann, F.: Towards closing the gap between hygroscopic growth and activation for secondary organic aerosol – Part 2: Theoretical approaches, Atmos. Chem. Phys., 9, 3999–4009, doi:10.5194/acp-9-3999-2009, 2009.

Pratt, K. A. and Prather, K. A.: Aircraft measurements of vertical profiles of aerosol mixing states, J. Geophys. Res., 115, D11305, doi:10.1029/2009jd013150, 2010.

Rader, D. J. and McMurry, P. H.: Application of the tandem differential mobility analyser to

ACPD
11, 2991–3040, 2011

studies of droplet growth or evaporation, J. Aerosol Sci., 17, 771–787, 1986.
Riemer, N., West, M., Zaveri, R. A., and Easter, R. C.: Simulating the evolution of soot mixing state with a particle-resolved aerosol model, J. Geophys. Res., 114, D09202, doi:10.1029/2008jd011073, 2009.
Riemer, N., West, M., Zaveri, R., and Easter, R.: Estimating black carbon aging time-scales with a particle-resolved aerosol model, J. Aerosol Sci., 41, 143–158, 2010.
Rissler, J., Vestin, A., Swietlicki, E., Fisch, G., Zhou, J., Artaxo, P., and Andreae, M. O.: Size distribution and hygroscopic properties of aerosol particles from dry-season biomass burning in Amazonia, Atmos. Chem. Phys., 6, 471–491, doi:10.5194/acp-6-471-2006, 2006.
Sjogren, S., Gysel, M., Weingartner, E., Alfarra, M. R., Duplissy, J., Cozic, J., Crosier, J., Coe, H., and Baltensperger, U.: Hygroscopicity of the submicrometer aerosol at the high-alpine site Jungfraujoch, 3580 m a.s.l., Switzerland, Atmos. Chem. Phys., 8, 5715–5729, doi:10.5194/acp-8-5715-2008, 2008.
Skamarock, W. C., Klemp, J. B., Dudhia, J., Gill, D. O., Barker, D. M., Wang, W., and Powers, J. G.: A Description of the Advanced Research WRF Version 2, Tech. Rep. NCAR/TN-468+STR, NCAR, 2005.
Stolzenburg, M. R. and McMurry, P. H.: TDMAfit user's manual, University of Minnesota, Department of Mechanical Engineering, Particle Technology Laboratory, 1–80, Minneapolis, 1988.
Stratmann, F., Kiselev, A., Wurzler, S., Wendisch, M., Heintzenberg, J., Charlson, R. J., Diehl, K., Wex, H., and Schmidt, S.: Laboratory studies and numerical simulations of cloud droplet formation under realistic supersaturation conditions, J. Atmos. Ocean. Tech., 21, 876–887, 2004.
Su, H., Rose, D., Cheng, Y. F., Gunthe, S. S., Massling, A., Stock, M., Wiedensohler, A., Andreae, M. O., and Pöschl, U.: Hygroscopicity distribution concept for measurement data analysis and modeling of aerosol particle mixing state with regard to hygroscopic growth and CCN activation, Atmos. Chem. Phys., 10, 7489–7503, doi:10.5194/acp-10-7489-2010, 2010.
Svenningsson, B., Hansson, H.-C., Wiedensohler, A., Noone, K., Ogren, J., Hallberg, A., and Colvile, R.: Hygroscopic growth of aerosol particles and its influence on nucleation scavenging in cloud: Experimental results from Kleiner Feldberg, J. Atmos. Chem., 19, 129–152, 1994.
Swietlicki, E., Zhou, J., Berg, O. H., Martinsson, B. G., Frank, G., Cederfelt, S.-I., Dusek, U.,

ACPD
11, 2991–3040, 2011

Berner, A., Birmili, W., Wiedensohler, A., Yuskiewicz, B., and Bower, K. N.: A closure study of sub-micrometer aerosol particle hygroscopic behaviour, Atmos. Res., 50, 205–240, 1999.
Swietlicki, E., Hansson, H.-C., Hämeri, K., Svenningsson, B., Massling, A., Mcfiggans, G., Mcmurry, P. H., Petäjä, T., Tunved, P., Gysel, M., Topping, D., Weingartner, E., Baltensperger, U., Rissler, J., Wiedensohler, A., and Kulmala, M.: Hygroscopic properties of submicrometer atmospheric aerosol particles measured with H-TDMA instruments in various environments: a review, Tellus B, 60, 432–469, 2008.
Topping, D. O., McFiggans, G. B., and Coe, H.: A curved multi-component aerosol hygroscopicity model framework: Part 1 – Inorganic compounds, Atmos. Chem. Phys., 5, 1205–1222, doi:10.5194/acp-5-1205-2005, 2005a.
Topping, D. O., McFiggans, G. B., and Coe, H.: A curved multi-component aerosol hygroscopicity model framework: Part 2 – Including organic compounds, Atmos. Chem. Phys., 5, 1223–1242, doi:10.5194/acp-5-1223-2005, 2005b.
Tuch, T. M., Haudek, A., Müller, T., Nowak, A., Wex, H., and Wiedensohler, A.: Design and performance of an automatic regenerating adsorption aerosol dryer for continuous operation at monitoring sites, Atmos. Meas. Tech., 2, 417–422, doi:10.5194/amt-2-417-2009, 2009.
Twomey, S.: Pollution and the planetary albedo, Atmos. Environ., 8, 1251–1256, 1974.
Wehner, B., Wiedensohler, A., Tuch, T. M., Wu, Z. J., Hu, M., Slanina, J., and Kiang, C. S.: Variability of the aerosol number size distribution in Beijing, China: New particle formation, dust storms, and high continental background, Geophys. Res. Lett., 31, L22108, doi:10.1029/2004gl021596, 2004.
Wehner, B., Birmili, W., Ditas, F., Wu, Z., Hu, M., Liu, X., Mao, J., Sugimoto, N., and Wiedensohler, A.: Relationships between submicrometer particulate air pollution and air mass history in Beijing, China, 20042006, Atmos. Chem. Phys., 8, 6155–6168, doi:10.5194/acp-8-6155-2008, 2008.
Wex, H., Kiselev, A., Ziese, M., and Stratmann, F.: Calibration of LACIS as a CCN detector and its use in measuring activation and hygroscopic growth of atmospheric aerosol particles, Atmos. Chem. Phys., 6, 4519–4527, doi:10.5194/acp-6-4519-2006, 2006.
Wex, H., Hennig, T., Salma, I., Ocskay, R., Kiselev, A., Henning, S., Massling, A., Wiedensohler, A., and Stratmann, F.: Hygroscopic growth and measured and modeled critical super-saturations of an atmospheric HULIS sample, Geophys. Res. Lett., 34, L02818, doi:10.1029/2006gl028260, 2007.
Wex, H., Petters, M. D., Carrico, C. M., Hallbauer, E., Massling, A., McMeeking, G. R., Poulain,

ACPD
11, 2991–3040, 2011

L., Wu, Z., Kreidenweis, S. M., and Stratmann, F.: Towards closing the gap between hygroscopic growth and activation for secondary organic aerosol: Part 1 – Evidence from measurements, Atmos. Chem. Phys., 9, 3987–3997, doi:10.5194/acp-9-3987-2009, 2009.

Young, K. C. and Warren, A. J.: A reexamination of the derivation of the equilibrium supersaturation curve for soluble particles, J. Atmos. Sci., 49, 1138–1143, 1992.

Zaveri, R. A., Easter, R. C., Fast, J. D., and Peters, L. K.: Model for simulating aerosol interactions and chemistry (MOSAIC), J. Geophys. Res., 113, D13204, doi:10.1029/2007jd008782, 2008.

Zhang, R., Khalizov, A. F., Pagels, J., Zhang, D., Xue, H., and McMurry, P. H.: Variability in morphology, hygroscopicity, and optical properties of soot aerosols during atmospheric processing, Proc. Natl. Acad. Sci., 105, 10291–10296, 2008.

Zhang, Q. H., Zhang, J. P., and Xue, H. W.: The challenge of improving visibility in Beijing, Atmos. Chem. Phys., 10, 7821–7827, doi:10.5194/acp-10-7821-2010, 2010.

Zhao, C., Tie, X., Brasseur, G., Noone, K. J., Nakajima, T., Zhang, Q., Zhang, R., Huang, M., Duan, Y., Li, G., and Ishizaka, Y.: Aircraft measurements of cloud droplet spectral dispersion and implications for indirect aerosol radiative forcing, Geophys. Res. Lett., 33, L16809, doi:10.1029/2006gl026653, 2006a.

Zhao, C., Tie, X., and Lin, Y.: A possible positive feedback of reduction of precipitation and increase in aerosols over Eastern Central China, Geophys. Res. Lett., 33, L11814, doi:10.1029/2006gl025959, 2006b.

ACPD
11, 2991–3040, 2011

Table 1. Summary of the HH-TDMA measurements of hygroscopic growth at 90%, 95% and 98.5% RH during HaChi summer campaign.

Dry diameter (nm)	50			100			200			250		
RH (%)	90	95	98.5	90	95	98.5	90	95	98.5	90	95	98.5
Number of scans	226	218	205	758	320	416	244	221	218	168	156	151
Inversion resolution ΔGF	0.075	0.075	0.10	0.075	0.075	0.125	0.075	0.075	0.125	0.075	0.075	0.125
Number fraction of GF < 1.2 group	0.22±0.14	0.13±0.11	0.07±0.08	0.16±0.10	0.14±0.09	0.09±0.08	0.16±0.09	0.14±0.09	0.10±0.08	0.15±0.10	0.13±0.09	0.09±0.09
Nearly-hydrophobic group, NH												
Number fraction	0.18±0.12	0.20±0.13	0.17±0.13	0.16±0.10	0.18±0.11	0.15±0.11	0.16±0.09	0.16±0.10	0.12±0.10	0.15±0.10	0.14±0.10	0.11±0.10
Mean GF ± std (when present)	1.10±0.03	1.16±0.04	1.25±0.08	1.08±0.02	1.13±0.06	1.24±0.13	1.07±0.02	1.10±0.05	1.17±0.14	1.06±0.02	1.09±0.04	1.15±0.15
Mean spread σ of GF	0.04±0.01	0.07±0.02	0.11±0.03	0.05±0.01	0.07±0.02	0.14±0.06	0.04±0.01	0.06±0.03	0.12±0.07	0.04±0.01	0.05±0.02	0.10±0.06
Mean κ± std	0.054±0.014	0.051±0.013	0.049±0.017	0.034±0.011	0.032±0.016	0.031±0.019	0.028±0.010	0.021±0.012	0.016±0.016	0.025±0.007	0.018±0.010	0.013±0.017
Mean spread σ of κ	0.023±0.005	0.024±0.006	0.023±0.007	0.023±0.006	0.022±0.008	0.021±0.009	0.018±0.005	0.015±0.007	0.013±0.009	0.016±0.005	0.012±0.007	0.010±0.007
More-hygroscopic group, MH												
Number fraction	0.68±0.18	0.66±0.18	0.69±0.17	0.78±0.12	0.75±0.13	0.79±0.14	0.81±0.11	0.82±0.12	0.85±0.13	0.84±0.12	0.84±0.12	0.87±0.11
Mean GF ± std	1.46±0.05	1.68±0.06	2.13±0.09	1.54±0.02	1.81±0.04	2.45±0.07	1.61±0.04	1.94±0.05	2.74±0.09	1.63±0.04	1.98±0.05	2.81±0.09
Mean spread σ of GF	0.051±0.013	0.065±0.016	0.117±0.026	0.055±0.011	0.069±0.012	0.125±0.023	0.061±0.010	0.082±0.013	0.142±0.019	0.060±0.011	0.081±0.013	0.140±0.018
Mean κ ± std	0.31±0.04	0.30±0.04	0.31±0.04	0.33±0.02	0.32±0.02	0.33±0.03	0.38±0.03	0.37±0.03	0.38±0.04	0.39±0.03	0.39±0.03	0.39±0.04
Mean spread σ of κ	0.045±0.012	0.041±0.011	0.048±0.011	0.045±0.009	0.042±0.008	0.047±0.009	0.054±0.009	0.053±0.009	0.057±0.009	0.054±0.010	0.054±0.009	0.058±0.009
Ensemble mean of all groups												
Mean GF ± std	1.39±0.07	1.57±0.10	1.97±0.15	1.48±0.05	1.70±0.08	2.31±0.12	1.54±0.06	1.84±0.09	2.61±0.14	1.57±0.06	1.89±0.08	2.70±0.13
Mean spread σ of GF	0.14±0.04	0.20±0.06	0.32±0.11	0.17±0.05	0.25±0.08	0.42±0.17	0.20±0.05	0.29±0.08	0.47±0.20	0.20±0.06	0.29±0.10	0.45±0.22
Mean κ ± std	0.25±0.06	0.24±0.06	0.25±0.06	0.28±0.04	0.26±0.04	0.28±0.04	0.32±0.04	0.31±0.05	0.33±0.05	0.34±0.05	0.33±0.05	0.35±0.05
Mean spread σ of κ	0.10±0.03	0.10±0.03	0.10±0.03	0.11±0.03	0.11±0.03	0.11±0.04	0.13±0.03	0.13±0.03	0.12±0.04	0.13±0.04	0.13±0.04	0.12±0.05

ACPD
11, 2991–3040, 2011

Table 2. Summary of fitting parameters for the parameterization of κ and nf; see Eq. (13) and Sect. 3.4 for description.

	B	C	D
Summer daytime scans			
κ more-hygroscopic group	−0.150	0.000703	0.553
κ nearly-hydrophobic group	−0.0391	-4.12×10^{-6}	0.121
κ all groups	−0.172	0.000807	0.553
nf more-hygroscopic group	−0.0930	0.000664	0.963
nf nearly-hydrophobic group	0.0886	−0.000337	−0.0596
Summer nighttime scans			
κ more-hygroscopic group	0.0837	0.000228	0.144
κ nearly-hydrophobic group	−0.0926	0.000158	0.200
κ all groups	0.136	8.00×10^{-5}	−0.0101
nf more-hygroscopic group	0.644	−0.00129	−0.408
nf nearly-hydrophobic group	−0.166	0.000313	0.491
Summer average			
κ more-hygroscopic group	0.0285	0.000320	0.243
κ nearly-hydrophobic group	−0.0812	0.000126	0.183
κ all groups	0.0533	0.000279	0.141
nf more-hygroscopic group	0.431	−0.000682	−0.0196
nf nearly-hydrophobic group	−0.0770	3.09×10^{-5}	0.314

ACPD
11, 2991–3040, 2011

Table 3. Schemes used in different cases of the PartMC-MOSAIC simulation.

Case no.	Coagulation	Gas, particle phase chemistries	Mixing layer height
c1	off	off	varied
c2	on	off	varied
c3	on	on	varied
c4	on	on	fixed (1000 m)

ACPD
11, 2991–3040, 2011

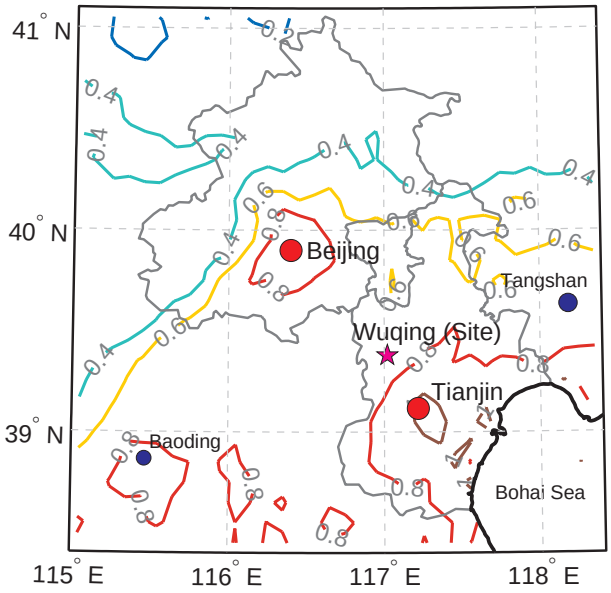

Fig. 1. Map shows the site location (magenta star), major cities in the vicinity (red and blue circles) and contour lines of the 4-yr average MODIS AOD (Aerosol Optical Depth) distribution (2005–2008, $0.1^\circ \times 0.1^\circ$ resolution).

ACPD
11, 2991–3040, 2011

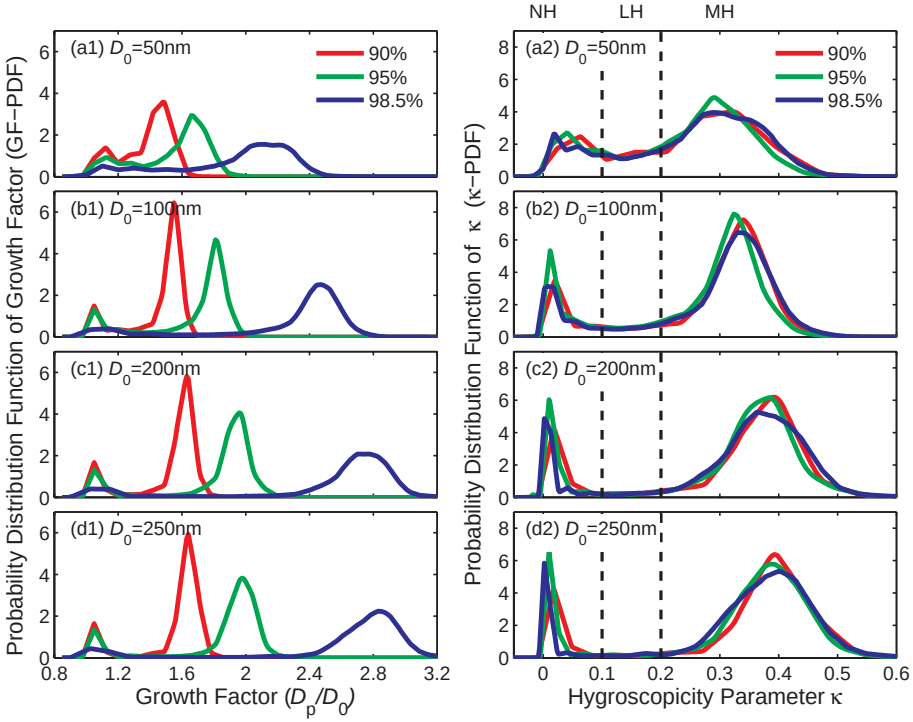

Fig. 2. Averaged probability distribution functions of **(a1)–(d1)** growth factor (GF-PDF); **(a2)–(d2)** hygroscopicity parameter κ (κ-PDF); dashed lines represent the boundaries of the three defined hygroscopic groups; data were averaged over the whole period of HaChi summer campaign.

ACPD
11, 2991–3040, 2011

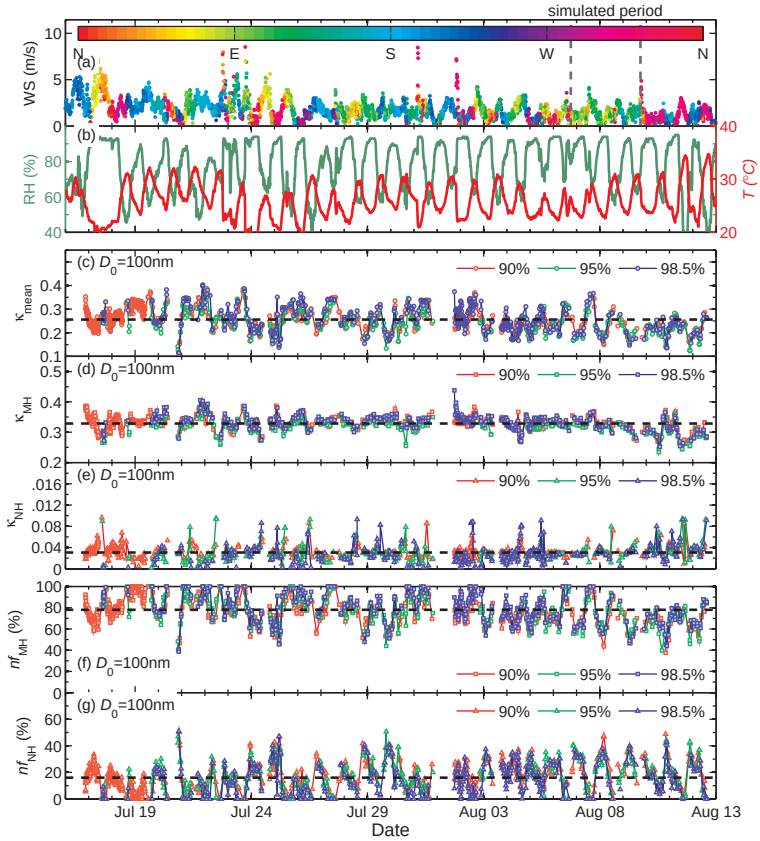

Fig. 3. Time series of meteorological parameters and hygroscopic properties of 100 nm particles in the HaChi summer campaign. **(a)** wind speed and wind direction; **(b)** temperature (T) and relative humidity (RH); **(c)** mean κ (averaged over both modes, 100 nm dry diameter); **(d)** κ of more-hygroscopic group particles; **(e)** κ of nearly-hydrophobic mode particles; **(f)** number fraction of more-hygroscopic group particles; **(g)** number fraction of nearly-hydrophobic group.

ACPD
11, 2991–3040, 2011

Hygroscopic properties of aerosol particles at high RH

P. F. Liu et al.

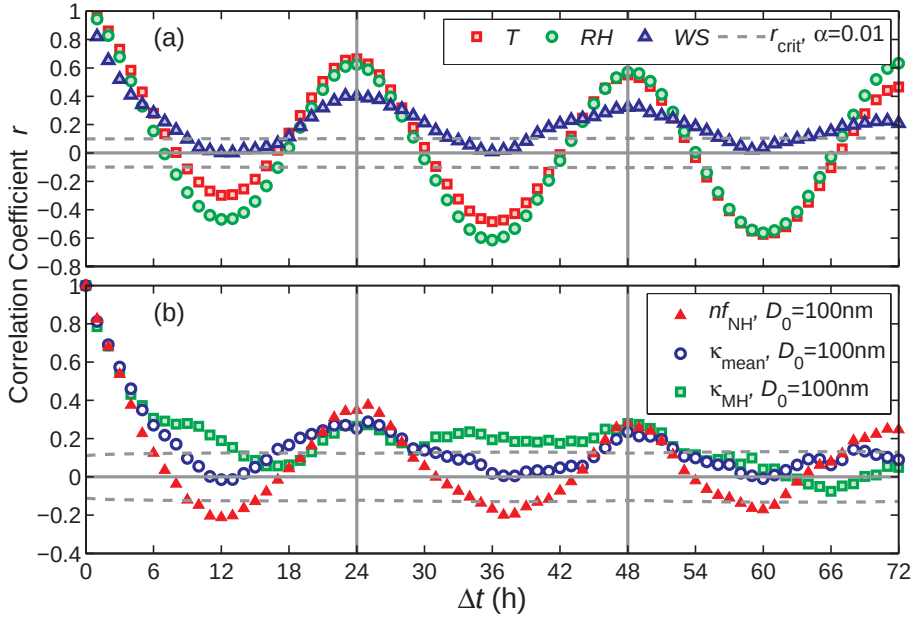

Fig. 4. Autocorrelation analysis of meteorological parameters and hygroscopic properties of 100 nm particles. **(a)** temperature (T), relative humidity (RH) and wind speed (WS); **(b)** number fraction of nearly-hydrophobic group (nf_{NH}), mean κ (κ_{mean}) and κ of more hygroscopic group (κ_{MH}). The dashed lines show the significance level of 0.01.

ACPD
11, 2991–3040, 2011

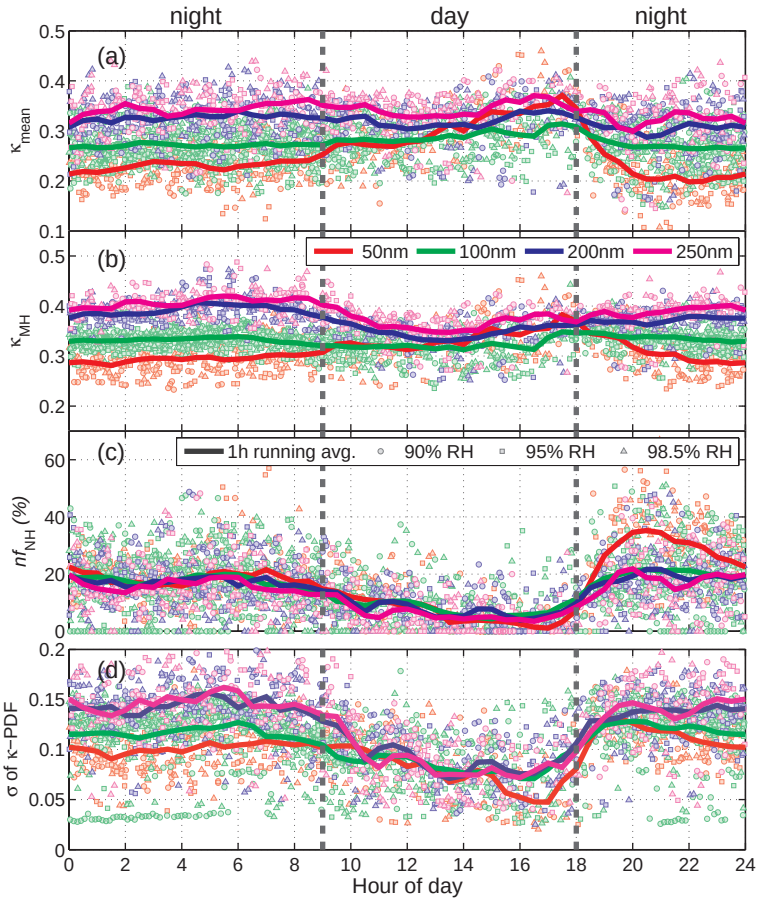

Fig. 5. Diurnal variations of aerosol hygroscopic properties; **(a)** mean κ of all groups; **(b)** κ of more-hygroscopic group; **(c)** the number fraction of nearly-hydrophobic group; **(d)** the spread of κ-PDF.

ACPD
11, 2991–3040, 2011

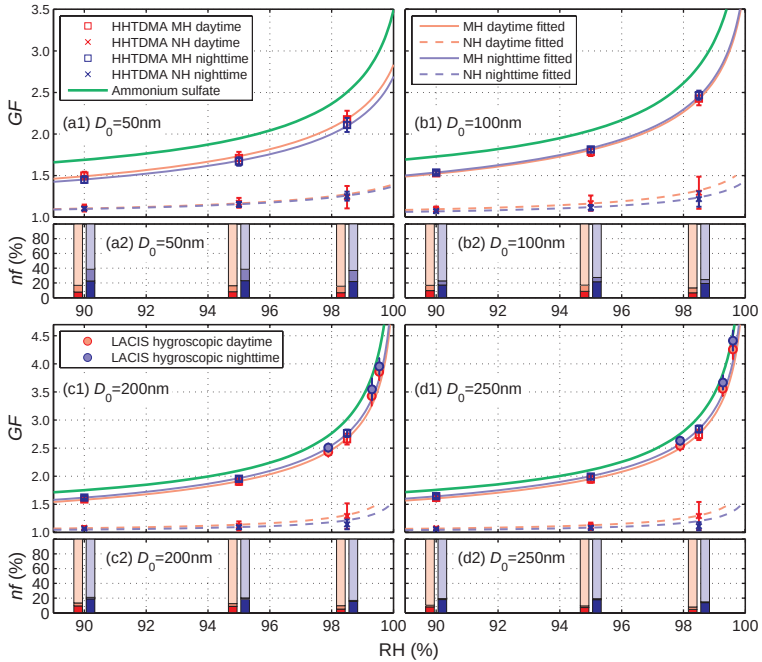

Fig. 6. **(a1)–(d1)** The hygroscopic growth of aerosol particles with different dry diameters of 50 nm, 100 nm, 200 nm and 250 nm, respectively. The growth factors (GF) of nearly-hydrophobic (NH) group and more-hygroscopic (MH) group are the mean values of the measured GFs corrected to their set RHs (90%, 95% and 98.5%); the error bars represent ±1 s.d.; the blue and red lines are fitted κ-Köhler curves using the mean κ measured by the HH-TDMA; the green lines are the hygroscopic growth of ammonium sulphate particles calculated following Low (1969) and Young and Warren (1992). **(a2)–(d2)** the mean number fractions of nearly-hydrophobic (NH) group, less-hygroscopic (LH) group and more-hygroscopic (MH) group particles (from dark colour to light colour) with 50 nm, 100 nm, 200 nm and 250 nm dry diameters.

ACPD
11, 2991–3040, 2011

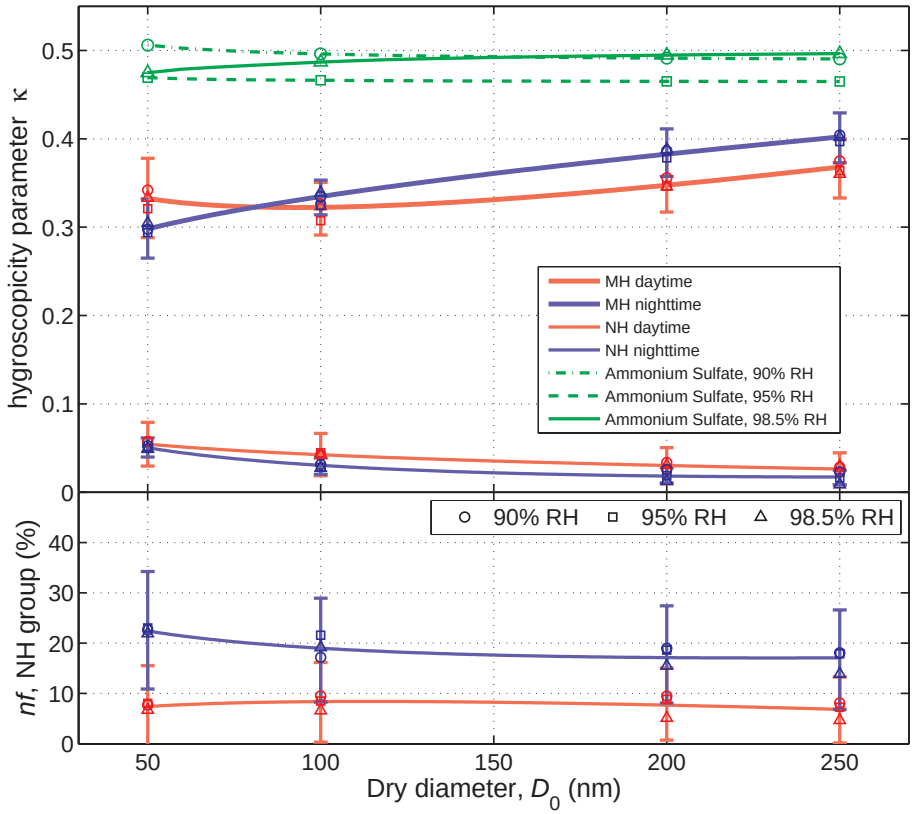

Fig. 7. Parameterization of κ and nf. The upper panel shows the parameterizations of κ as functions of dry diameter for more-hygroscopic group and nearly-hydrophobic group particles during the day and during the night, respectively; the lower panel shows the parameterizations of the number fractions of nearly-hydrophobic group particles.

ACPD
11, 2991–3040, 2011

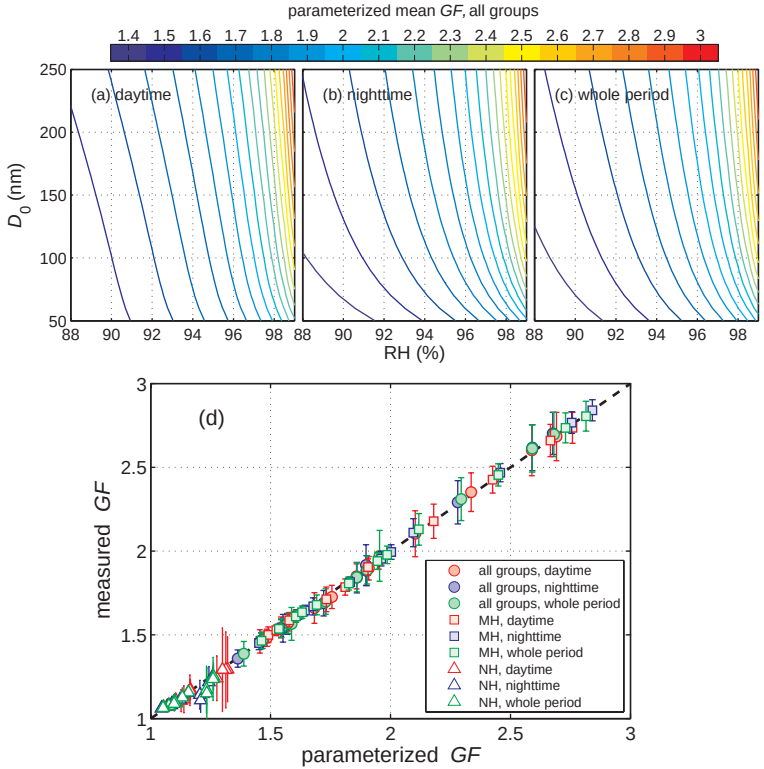

Fig. 8. Contours show the parameterized mean growth factors of all groups during **(a)** daytime; **(b)** nighttime; **(c)** whole period of HaChi summer campaign. **(d)** Comparison between measured and parameterized growth factors; the error bars represent the one standard deviation of the measurements during the summer campaign period; the dashed line shows the 1:1 line.

ACPD
11, 2991–3040, 2011

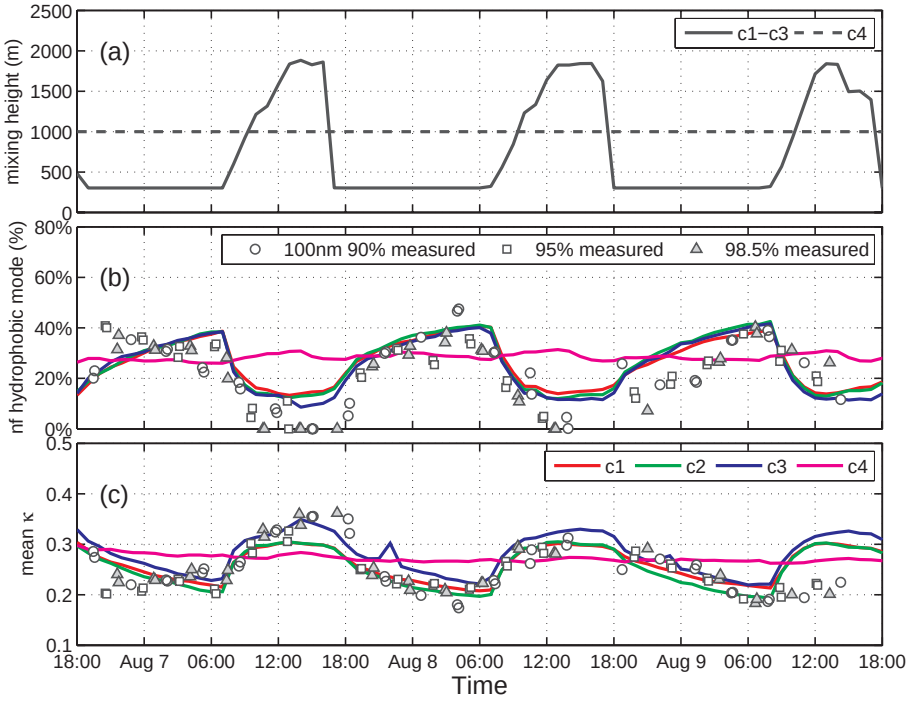

Fig. 9. Comparisons between the PartMC-MOSAIC simulations and the HH-TDMA measurements. **(a)** Mixing layer height set for different cases; **(b)** number fraction of nearly-hydrophobic particles; **(c)** mean hygroscopicity parameter κ of all groups. See Table 3 for the settings in the model for the four cases c1–c4.

ACPD
11, 2991–3040, 2011